Eur J Nucl Med Mol Imaging (2013) 40:125–132
DOI 10.1007/s00259-012-2261-2

ORIGINAL ARTICLE

Comparison of the binding characteristics of [^{18}F]THK-523 and other amyloid imaging tracers to Alzheimer's disease pathology

Ryuichi Harada · Nobuyuki Okamura · Shozo Furumoto · Tetsuro Tago · Masahiro Maruyama · Makoto Higuchi · Takeo Yoshikawa · Hiroyuki Arai · Ren Iwata · Yukitsuka Kudo · Kazuhiko Yanai

Received: 1 May 2012 / Accepted: 21 September 2012 / Published online: 26 October 2012

Abstract
Purpose Extensive deposition of senile plaques and neurofibrillary tangles in the brain is a pathological hallmark of Alzheimer's disease (AD). Although several PET imaging agents have been developed for in vivo detection of senile plaques, no PET probe is currently available for selective detection of neurofibrillary tangles in the living human brain. Recently, [^{18}F]THK-523 was developed as a potential in vivo imaging probe for tau pathology. The purpose of this study was to compare the binding properties of [^{18}F]THK-523 and other amyloid imaging agents, including PiB, BF-227 and FDDNP, to synthetic protein fibrils and human brain tissue.
Methods In vitro radioligand binding assays were conducted using synthetic amyloid β_{42} and K18ΔK280-tau fibrils. Nonspecific binding was determined by the addition of unlabelled compounds at a concentration of 2 μM. To examine radioligand binding to neuropathological lesions, in vitro autoradiography was conducted using sections of AD brain.
Results [^{18}F]THK-523 showed higher affinity for tau fibrils than for Aβ fibrils, whereas the other probes showed a higher affinity for Aβ fibrils. The autoradiographic analysis indicated that [^{18}F]THK-523 accumulated in the regions containing a high density of tau protein deposits. Conversely, PiB and BF-227 accumulated in the regions containing a high density of Aβ plaques.
Conclusion These findings suggest that the unique binding profile of [^{18}F]THK-523 can be used to identify tau deposits in AD brain.

Keywords PET probes · Tau · Amyloid · Alzheimer's disease

Electronic supplementary material The online version of this article (doi:10.1007/s00259-012-2261-2) contains supplementary material, which is available to authorized users.

R. Harada · N. Okamura (✉) · S. Furumoto · T. Yoshikawa · K. Yanai
Department of Pharmacology,
Tohoku University School of Medicine,
2-1, Seiryo-machi, Aoba-ku,
Sendai 980-8575, Japan
e-mail: nookamura@med.tohoku.ac.jp

S. Furumoto · T. Tago · R. Iwata
Division of Radiopharmaceutical Chemistry,
Cyclotron and Radioisotope Center, Tohoku University,
Sendai, Japan

M. Maruyama · M. Higuchi
Molecular Imaging Center, National Institute
of Radiological Sciences,
Chiba, Japan

H. Arai
Department of Geriatrics and Gerontology, Institute of
Development, Aging and Cancer, Tohoku University,
Sendai, Japan

Y. Kudo
Innovation of New Biomedical Engineering Center,
Tohoku University,
Sendai, Japan

Introduction

Senile plaques and neurofibrillary tangles (NFTs) composed of amyloid-β (Aβ) peptides and aggregated tau proteins, respectively, are the pathological hallmarks of

Alzheimer's disease (AD). In vivo amyloid imaging techniques have received a lot of attention for their promise in presymptomatic detection of Aβ pathology [1]. Recently, several β-sheet binding radiotracers have been developed as PET amyloid imaging agents [2]. Among them, ^{18}F-labelled 2-(1-{6-[(2-fluoroethyl(methyl)amino)-2-naphthyl)ethylidene)malononitrile ([^{18}F]FDDNP) was the first PET probe to be applied to clinical PET imaging in patients with AD [3]. This tracer demonstrated higher regional uptake in the medial temporal lobe and neocortex, and was claimed to bind to Aβ and tau pathological lesions [3]. Subsequently, ^{11}C-labelled 2-[4′-(methylamino)phenyl]-6-hydroxybenzothiazole ([^{11}C]PiB) and 2-(2-[dimethylaminothiazole-5-yl]ethenyl)-6-(2-[fluoro]ethoxy)benzoxazole ([^{11}C]BF-227) were also developed as amyloid imaging radiotracers. These tracers bind to Aβ fibrils with high affinity [4] and have demonstrated a significantly higher retention in the neocortical areas of brains of AD patients than of healthy controls [5, 6]. Furthermore, post-mortem analysis of AD patients who had undergone [^{11}C]PiB PET imaging before death suggested a strong correlation between in vivo PiB binding and regional distribution of Aβ plaques [7].

Amyloid imaging with PET can detect AD pathology in its preclinical stage [8]. However, amyloid deposition as assessed by [^{11}C]PiB PET correlates poorly with cognitive impairment in AD [9, 10], whereas deposition of tau in the medial temporal cortex is closely associated with neuronal death in this region. Selective tau imaging would provide important information about the tau pathophysiological features in AD, allowing correlation of brain tau load with cognitive decline, monitoring of disease progression and evaluation of therapeutic efficacy of newly developed therapies. Potential candidates for in vivo tau imaging agents include quinoline derivatives [11], and in a recent study, we found that one quinoline derivative, [^{18}F]THK-523, showed higher affinity for tau rather than amyloid fibrils. Furthermore, an autoradiography analysis indicated that this tracer binds specifically to tau deposits but not Aβ burden at tracer concentrations usually achieved during a PET scan [12].

The binding profiles of PiB, BF-227 and FDDNP to Aβ fibrils have been well described. Because tau, α-synuclein and prion fibrils, as well as Aβ fibrils, share a common β-sheet secondary structure, these compounds can potentially bind all these misfolded proteins. A previous study indicated that PiB binds to both Aβ and PHF tau pathology in vitro [13]. However, the binding occurs at higher concentrations than usually achieved in vivo during a PET scan. Furthermore, PET–pathology correlation studies have demonstrated that PiB binding reflects Aβ pathology [7, 14]. Newly developed ^{18}F-labelled amyloid PET tracers have similarly shown good correlation with Aβ plaque density [15, 16]. However, the binding affinity of these radiotracers for tau fibrils remains unknown and the binding properties of [^{18}F]THK-523 have not been directly compared with those of other amyloid PET agents. Here, we compared the binding affinity of [^{18}F]THK-523 to synthetic Aβ and tau protein fibrils as well as to senile plaques and NFTs in human brain samples with those of PiB, BF-227 and FDDNP, to characterize the binding properties of THK-523 and to obtain a better understanding of current and future PET data.

Materials and methods

Materials

The nonlabelled compounds PiB, BF-227, FDDNP, THK-523 (Fig. 1) and their precursors were custom-synthesized by Tanabe R&D Service (Osaka, Japan). Human $A\beta_{42}$ was purchased from Peptide Institute Inc. (Mino, Japan). Recombinant K18ΔK280-tau protein was obtained from Invitrogen (Tokyo, Japan).

Radiolabelling of PiB, BF-227, THK-523 and FDDNP

[^{3}H]PiB (specific activity 2.96 GBq/μmol) was purchased from American Radiolabeled Chemicals (St. Louis, MO). [^{11}C]PiB was radiolabelled using its precursor (2-(4-aminophenyl)-6-methoxymethoxybenzothiazole) and [^{11}C]methyl triflate, as

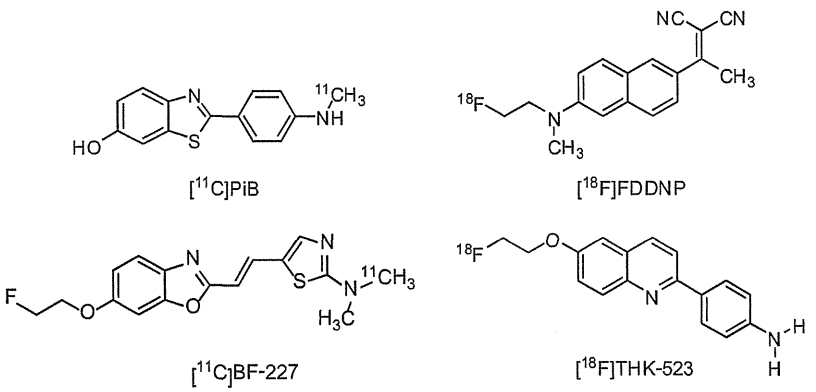

Fig. 1 Chemical structures of [^{11}C]PiB, [^{18}F]FDDNP, [^{11}C]BF-227 and [^{18}F]THK-523

previously described [17, 18]. The mean specific activity of [^{11}C]PiB was 34.6 GBq/μmol.

[^{18}F]BF-227 was synthesized by nucleophilic substitution of the tosylate precursor (2-[2-(2-dimethylaminothiazol-5-yl)ethenyl]-6-[2-(tosyloxy)ethoxy]benzoxazole. After a 10-min reaction at 110 °C, the crude mixture was partially purified on an activated Sep-Pak tC18 cartridge before being purified by semi-preparative reverse-phase HPLC. Standard tC18 Sep-Pak reformulation produced [^{18}F]BF-227 in >95 % purity. The radiochemical yield was 12–19 % (non-decay-corrected), and the mean specific activity of [^{18}F]BF-227 was 163 GBq/μmol at the end of the synthesis. [^{11}C]BF-227 was synthesized using *N*-desmethylated derivatives as its precursor and [^{11}C]methyl triflate, as previously described [6]. The mean specific activity of [^{11}C]BF-227 was 136 GBq/μmol.

[^{18}F]THK-523 was synthesized by nucleophilic substitution of the tosylate precursor (2-(4-aminophenyl)-6-(2-tosyloxyethoxy)quinolone) as previously described [12]. The standard tC18 Sep-Pak reformulation produced [^{18}F]THK-523 in >95 % purity. The radiochemical yield was 38–49 % (non-decay-corrected), and the mean specific activity of [^{18}F]THK-523 was 68 GBq/μmol at the end of the synthesis.

[^{18}F]FDDNP was radiolabelled by the nucleophilic substitution of the tosylate precursor (2-{[6-(2,2-dicyano-1-methylvinyl)-2-naphthyl](methyl)amino}ethyl-4-methylbenzenesulphonate) as previously described [19]. After a 15-min reaction at 95 °C, the crude mixture was partially purified on an activated Sep-Pak tC18 cartridge before being purified by semipreparative reverse-phase HPLC. Standard tC18 Sep-Pak reformulation produced [^{18}F]FDDNP in >95 % purity. The radiochemical yield was 12–19 % (non-decay-corrected), and the mean specific activity of [^{18}F]FDDNP was 27 GBq/μmol at the end of the synthesis. All analysis HPLC chromatograms are shown in the Supplementary figure.

In vitro radioligand binding assays

Synthetic $A\beta_{42}$ fibrils and K18ΔK280-tau fibrils were prepared as previously described [12]. For in vitro binding assays, synthetic $A\beta_{42}$ or K18ΔK280 fibrils (200 nM) were incubated with increasing concentrations of [^{3}H]PiB and ^{18}F-labelled compounds (0.5–200 nM). To account for nonspecific binding of [^{3}H]PiB and ^{18}F-labelled compounds, the above-mentioned reactions were performed in triplicate in the presence of each unlabelled compound at a concentration of 2 μM.

The binding reactions were incubated for 1 h for the ^{18}F-labelled compounds and 3 h for [^{3}H]PiB at room temperature, in 200 μL of assay buffer (Dulbecco's PBS, 0.1 % BSA). Separation of bound from free radioactivity was achieved by filtration under reduced pressure (MultiScreen HTS Vacuum Manifold, MultiScreen HTS 96-well 0.65-μm filtration plate; Millipore, Billerica, MA). The filters were washed three times with 200-μL assay buffer, and the filters containing the bound ^{18}F-labelled compounds were then assayed for radioactivity in a γ counter (AccuFLEX γ7000, Aloka, Tokyo, Japan). The filters containing [^{3}H]PiB were incubated in 2 mL of scintillation fluid (Aquasol-2; PerkinElmer, Boston, MA), and the radioactivity of ^{3}H was counted using a β counter (LS6500 liquid scintillation counter; Beckman Coulter, Brea, CA). The binding data were analysed with curve-fitting software that calculated the K_D and B_{max} using nonlinear regression (GraphPad Prism version 5.0; GraphPad Software, San Diego, CA).

Autoradiography, immunohistochemistry and Gallyas silver staining

Demographics of post-mortem brain samples are shown in Table 1. The frontal and medial temporal brain sections (6 μm thick) of three AD patients were incubated with 1.0 MBq/mL ^{11}C-labelled and ^{18}F-labelled compounds at room temperature for 10 min and then washed briefly with water and 50 % ethanol. After drying, the labelled sections were exposed to a BAS-III imaging plate (Fuji Film, Tokyo, Japan) overnight. The autoradiographic images were obtained using a BAS-5000 phosphoimaging instrument (Fuji Film) with a spatial resolution of 25×25 μm. The adjacent sections were immunostained using AT8 anti-tau monoclonal antibody (diluted 1:20; Innogenetics, Ghent, Belgium) and 6F/3D (diluted 1:50; Dako, Glostrup, Denmark). The adjacent sections were also stained by the Gallyas-Braak method, which has been reported to be NFT-specific [20].

Results

Binding affinity for synthetic Aβ and tau fibrils

To characterize the binding properties of THK-523, PiB, BF-227 and FDDNP, in vitro radioligand binding assays for synthetic $A\beta_{42}$ and truncated tau construct (K18ΔK280) fibrils were performed under the same experimental conditions. Truncated tau construct (K18ΔK280) consists of the four repeat regions (244–372) but lacking lysine 280 (ΔK280) observed in FTLD-17 familial mutation.

Table 1 Demographics of brain samples used in this study

Brain no.	Age (years)	Sex	Post-mortem interval (h)
AD1	76	F	16
AD2	82	F	17
AD3	92	F	8.5

K18ΔK280 tau aggregates exhibit the similar characteristic as PHF-tau from AD brain [21]. In addition, K18ΔK280 tau forms aggregates quickly without cofactor such as heparin [22]. Thus, we used K18ΔK280 fibrils for the in vitro binding assays. Our analysis indicated that [^{18}F]THK-523 had a higher binding affinity for tau fibrils (K_{D1} = 1.99 ± 0.21 nM, B_{max1} = 1.22 ± 0.24 pmol THK-523/nmol K18ΔK280-tau) than for $A\beta_{42}$ fibrils (K_{D1} = 30.3 ± 3.91 nM, B_{max1} = 12.6 ± 0.45 pmol THK-523/nmol $A\beta_{42}$), which was similar to previously published data [12]. On the other hand, [^{3}H]PiB bound to $A\beta_{42}$ fibrils with high affinity (K_{D1} = 0.84 ± 0.18 nM, B_{max1} = 0.44 ± 0.07 pmol PiB/nmol $A\beta_{42}$). [^{3}H]PiB also showed two binding sites for K18ΔK280-tau fibrils, but with a lower affinity (K_{D1} = 6.39 ± 1.63 nM, B_{max1} = 1.38 ± 0.48 pmol PiB/nmol K18ΔK280) than [^{18}F]THK-523. [^{18}F]BF-227 showed a high binding affinity for $A\beta_{42}$ fibrils (K_{D1} = 1.72 ± 0.83 nM, B_{max1} = 0.50 ± 0.14 pmol BF-227/nmol $A\beta_{42}$), similar to our previous report [23], but showed a lower affinity for tau fibrils (K_D = 30.2 ± 2.29 nM, B_{max} = 10.7 ± 0.24 pmol BF-227/nmol K18ΔK280-tau). [^{18}F]BF-227 had an approximately 20-fold higher affinity for the first class of $A\beta_{42}$ binding sites compared with tau fibrils. Only one class of [^{18}F]FDDNP binding site was identified on the $A\beta_{42}$ (K_D = 5.52 ± 1.97 nM, B_{max} = 0.277 ± 0.06 pmol FDDNP/nmol $A\beta_{42}$) and K18ΔK280 tau fibrils (K_D = 36.7 ± 11.6 nM, B_{max} = 2.14 ± 0.46 pmol FDDNP/nmol K18ΔK280-tau). These results suggest that [^{18}F]FDDNP binds $A\beta_{42}$ fibrils with lower affinity than [^{3}H]PiB and [^{18}F]BF-227. Furthermore, [^{18}F]FDDNP had an approximately sevenfold higher affinity for $A\beta_{42}$ fibrils than for tau fibrils. These binding profiles are significantly different from that of [^{18}F]THK-523 (Table 2).

In vitro autoradiography of human brain sections

To further assess the binding selectivity of [^{18}F]THK-523, autoradiographic images of the frontal (Fig. 2) and medial temporal (Fig. 3) brain sections from three AD patients, using [^{18}F]THK-523, [^{11}C]PiB and [^{11}C]BF-227, were compared. While Aβ plaques in the frontal grey matter were labelled with [^{11}C]PiB (Fig. 2a–c) and [^{11}C]BF-227 (Fig. 2g–i), the binding of [^{18}F]THK-523 in the frontal grey matter (Fig. 2m–o) was considerably lower. In the medial temporal brain sections, [^{11}C]PiB (Fig. 3a–c) and [^{11}C]BF-227 (Fig. 3g–i) did not accumulate in the hippocampal CA1 area, whereas [^{18}F]THK-523 (Fig. 3m–o) did accumulate in this area (Fig. 3m–o). The presence of a high density of tau and a low density of Aβ in this area was confirmed by immunohistochemistry (Fig. 3d–f, j–l). Furthermore, the band-like distribution of [^{18}F]THK-523 in the inner layer of the temporal grey matter was similar to the distribution of tau (Fig. 3j–l). In the high-magnification images of case AD3 (Fig. 3p–v), the distribution of [^{18}F]THK-523 closely resembled Gallyas silver staining and tau immunostaining. [^{18}F]THK-523 binding was observed in the areas showing a high density of NFTs in the hippocampal CA1, the layer pre-α and pri-α in the entorhinal cortex (ERC) (Fig. 3p, q, r, t). Intriguingly, [^{18}F]THK-523 labelling in the layer pre-α of the ERC corresponded to Gallyas silver staining better than tau immunostaining, suggesting the preferential binding of [^{18}F]THK-523 to extracellular tau deposits that were clearly visualized by Gallyas silver staining [25]. In contrast to [^{18}F]THK-523, the distribution of [^{11}C]PiB was similar to that of Aβ immunohistochemistry (Fig 3q, u, v). [^{11}C]PiB binding corresponded to the formation of amyloid in the parvopyramidal layer of the presubicular area and in the layers pre-β and pre-γ of the ERC (Fig. 3s, v) [26].

Discussion

In the study reported here, we for the first time directly compared the binding properties of the novel quinoline derivative THK-523 and other amyloid PET probes. Our data suggest the potential utility of THK-523 for the selective detection of PHF-tau in the living human brain, which has not previously been achieved. The autoradiographic images of sections from AD brains revealed that [^{18}F]THK-523 successfully labelled PHF-tau deposits but did not label Aβ deposits in the frontal and temporal cortices. These findings suggest that [^{18}F]THK-523 is a promising

Table 2 K_D and B_{max} values of [^{3}H]PiB, [^{18}F]BF-227, [^{18}F]FDDNP and [^{18}F]THK-523 for K18ΔK280-tau and $A\beta_{42}$ fibrils

Compound	K18ΔK280 fibrils				$A\beta_{42}$ fibrils			
	K_{D1}	B_{max1}	K_{D2}	B_{max2}	K_{D1}	B_{max1}	K_{D2}	B_{max2}
[^{18}F]THK-523	1.99±0.21	1.22±0.24	50.7±2.73	4.55±0.74	30.3±3.91	12.6±0.45	–	–
[^{18}F]BF-227	30.2±2.29	10.7±0.24	–	–	1.72±0.83	0.50±0.14	56.1±25.1	13.4±4.37
[^{18}F]FDDNP	36.7±11.6	2.14±0.46	–	–	5.52±1.97	0.277±0.06	–	–
[^{3}H]PiB	6.39±1.63	1.38±0.48	304±77.4	20.6±11.2	0.84±0.18	0.44±0.07	60.6±8.32	26.1±8.57

K_D values are in nanomoles, and B_{max} values are in picomoles compound per nanomole fibrils (n=3).

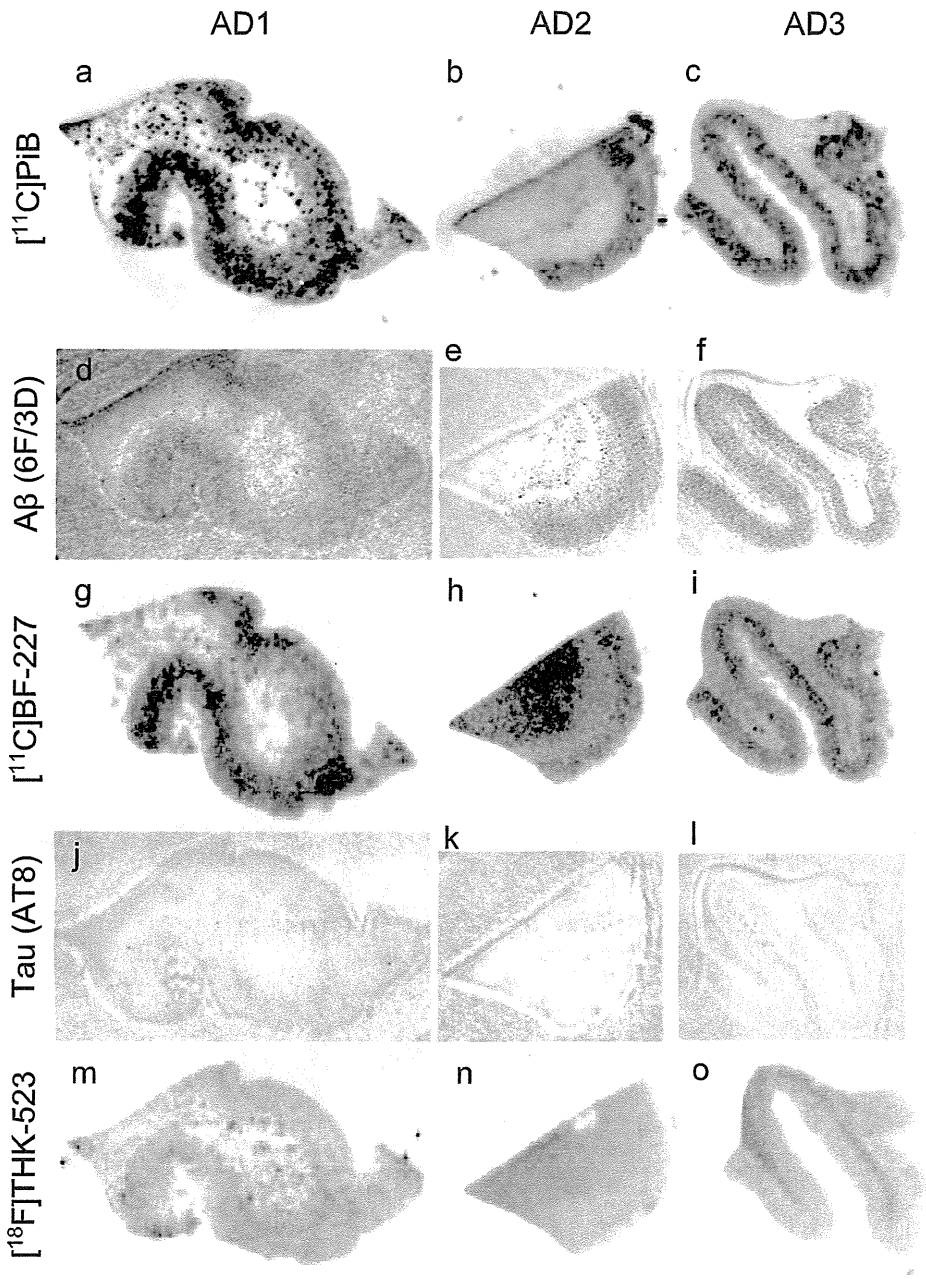

Fig. 2 Comparison of [^{11}C]PiB, [^{11}C]BF-227 and [^{18}F]THK-523 autoradiography with the Aβ and tau immunostaining in sections of the frontal brain from three patients with AD (*AD1*, *AD2*, *AD3*). Both [^{11}C]PiB (**a**–**c**) and [^{11}C]BF-227 (**g**–**i**) showed dense accumulation in the grey matter, closely resembling the pattern of Aβ immunohistochemistry using the 6F/3D antibody (**d**–**f**). [^{18}F]THK-523 (**m**–**o**) did not accumulate in the grey matter, which was correlated with no marked staining with anti-tau antibody AT8 (**j**–**l**)

candidate as a tau imaging tracer, and could also be a lead compound for future development of tau-selective radiotracers. We speculate that [^{18}F]THK-523 would show retention in tau-rich brain regions if administered to AD patients. However, the specific signal of [^{18}F]THK-523 might be lower than those of PiB and BF-227 owing to the lower amount of tau deposits in the neocortex of AD patients [27]. Further compound optimization may be required to achieve higher contrast imaging of PHF-tau deposits.

In in vitro saturation binding studies [^{18}F]THK-523 bound with higher affinity to tau fibrils (K_{D1} 1.99 nM) than to $A\beta_{42}$ fibrils (K_{D1} 30.3 nM), whereas PiB and BF-227 showed the opposite binding characteristics. [^{3}H]PiB bound with higher affinity to $A\beta_{42}$ fibrils (K_{D1} 0.84 nM) than to tau fibrils (K_{D1} 6.39 nM), similar to previous reports [7, 28, 29], and [^{18}F]BF-227 had more than a tenfold higher affinity for $A\beta_{42}$ fibrils (K_{D1} 1.72 nM) than for tau fibrils (K18ΔK280; K_{D1} 30.2 nM). Autoradiographic images of sections of AD brain revealed that [^{11}C]PiB and [^{11}C]BF-227 accumulated in the grey matter of the neocortex, which closely resembled the staining pattern of Aβ immunohistochemistry. A previous study suggested that [^{3}H]PiB labelled NFTs at tracer concentrations usually achieved during a PET scan [13]. However, another study showed no binding of the PiB derivative [^{3}H]BTA-1 to

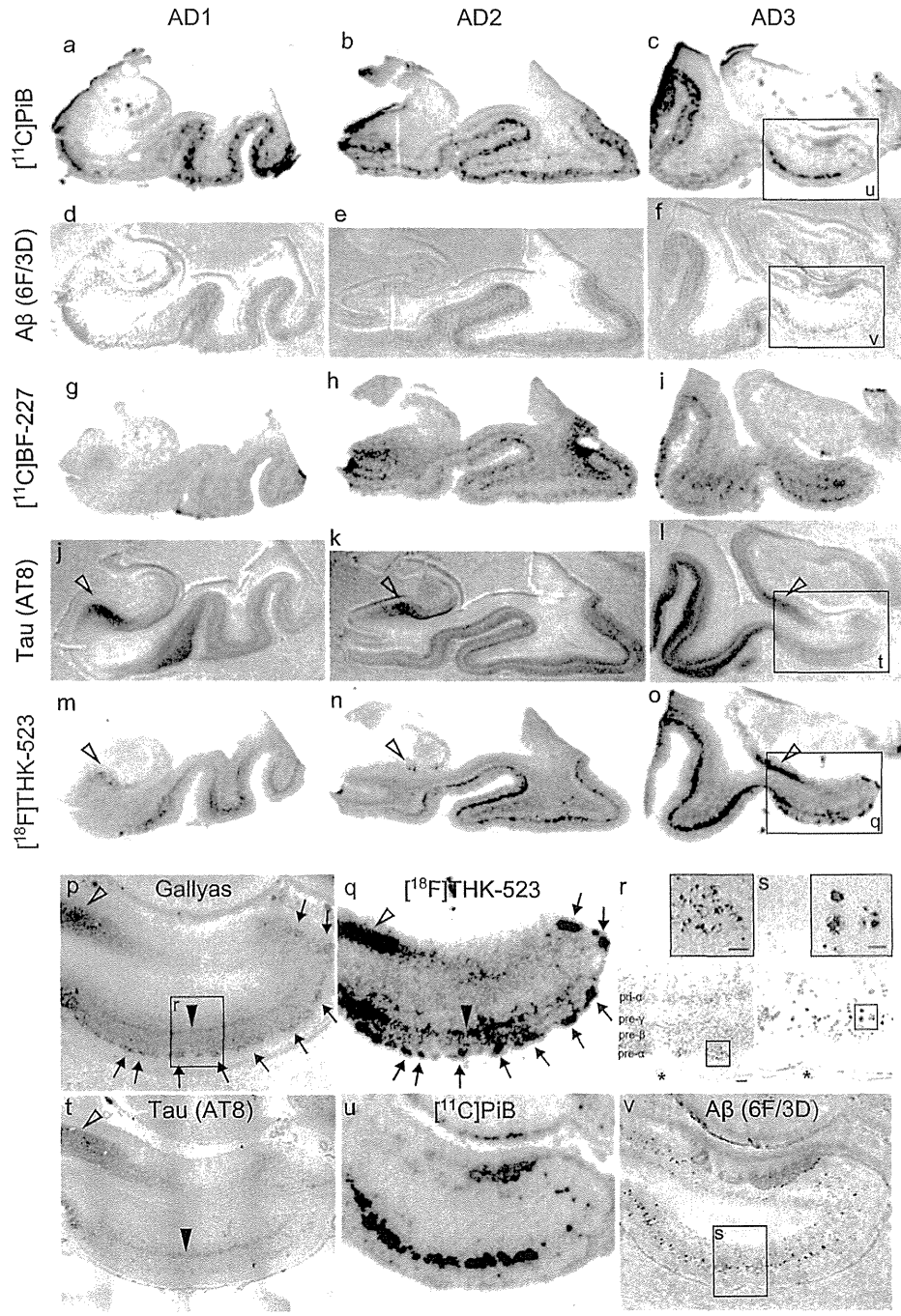

Fig. 3 Comparison of [^{11}C]PiB, [^{11}C]BF-227 and [^{18}F]THK-523 autoradiography with Aβ and tau immunostaining images in sections of the medial temporal brain from three patients with AD (*AD1*, *AD2*, *AD3*). [^{11}C]PiB (**a–c**) and [^{11}C]BF-227 (**g–i**) do not accumulate in the hippocampal CA1 area which contains a low density of Aβ (**d–f**). In contrast, accumulation of [^{18}F]THK-523 is observed in the hippocampal CA1 area (**m–o**, *arrowheads*), which closely resembles AT8 immunoreactivity (**j–l**, *arrowheads*). In addition, the band-like labelling pattern of [^{18}F]THK-523 in the inner layer of temporal cortex (**m–o**) is closely similar to that of AT8 immunostaining (**j–l**). **p–v** High magnification images of the medial temporal sections from patient AD3. Many clusters of [^{18}F]THK-523 binding in the ERC are consistent with Gallyas silver staining (**p**, **q**, *arrows*). **r** Close-up image from **p**. Numerous NFTs are located in the layer pre-α of the ERC (**r** *inset*). The band-like distribution of [^{18}F]THK-523 in the layer pri-α of the ERC also resembles the labelling pattern of Gallyas silver staining (**p**, *filled arrowhead*) as well as AT8 immunoreactivity (**t**, *filled arrowhead*). [^{11}C]PiB binding (**u**) is also present in the ERC, but obviously different from [^{18}F]THK-523 binding (**q**) and similar to the 6F/3D immunostaining pattern (**v**). Lake-like amyloid in the presubicular region (**v**) is labelled with [^{11}C]PiB, but not with [^{18}F]THK-523. **s** Close-up image from **v**. Aβ plaques (**s** *inset*) located in the layer pre-β and pre-γ are intensely labelled with [^{11}C]PiB (**u**). *Asterisks* in **r** and **s** denote the same large blood vessel. *Scale bar* 100 μm

plaque-free and NFT-rich ERC homogenates, despite the high amount of [^{3}H]BTA-1 binding to frontal cortex homogenates containing high levels of neuritic plaques [30]. Autoradiographic and immunohistochemical analyses indicated that PiB predominantly binds to senile plaques but not to NFTs. These findings are consistent with the findings from clinical PiB-PET studies showing no remarkable PiB retention in the medial temporal cortex of AD patients [7].

Another radiotracer, [^{18}F]FDDNP, has been reported to detect Aβ and tau pathological lesions in AD patients [3]. Previous clinical PET studies have shown higher cortical uptake of [^{18}F]FDDNP in the lateral and medial temporal lobes of AD subjects [3, 5]. Furthermore, a multitracer PET study of [^{11}C]PiB and [^{18}F]FDDNP has shown significant retention of FDDNP in the medial temporal cortex, albeit no remarkable retention of PiB in the same region [31]. However, in vitro binding studies have shown the limited binding affinity of [^{3}H]FDDNP to AD pathological lesions [24], and a previous autoradiographic analysis has suggested that [^{3}H]FDDNP does not significantly label any region in AD brain [24]. Previous in vitro binding studies additionally showed the binding affinity of FDDNP for $A\beta_{40}$ fibrils (K_D 0.12, 85 nM) [19, 24], but the binding affinity for tau fibrils was not reported. Here, we showed that the binding affinity of [^{18}F]FDDNP for tau fibrils (K_{D1} 36.7 nM) was similar to that of [^{18}F]BF-227 (K_{D1} 30.2 nM), but much higher than that of [^{18}F]THK-523 (K_{D1} 1.99 nM).

In conclusion, the binding profiles of [^{18}F]THK-523, [^{11}C]PiB, [^{18}F]BF-227, and [^{18}F]FDDNP were compared using in vitro saturation binding assays and autoradiography of sections of AD brain. These data suggest that [^{18}F]THK-523 shows a binding preference for tau protein fibrils. Therefore, [^{18}F]THK-523 is a candidate as a radiotracer to identify tau protein deposits and a lead compound for future tracer development. Ongoing clinical trials will clarify the clinical utility of this tracer and its derivatives for tau imaging in vivo.

Acknowledgments This study was supported by the Industrial Technology Research Grant Program of the NEDO in Japan, Health and Labor Sciences Research Grants from the Ministry of Health, Labor, and Welfare of Japan, and Grant-in-Aid for Scientific Research (B) (23390297).

References

1. Nordberg A, Rinne JO, Kadir A, Langstrom B. The use of PET in Alzheimer disease. Nat Rev Neurol. 2010;6:78–87. doi:10.1038/nrneurol.2009.217.
2. Furumoto S, Okamura N, Iwata R, Yanai K, Arai H, Kudo Y. Recent advances in the development of amyloid imaging agents. Curr Top Med Chem. 2007;7:1773–89.
3. Shoghi-Jadid K, Small GW, Agdeppa ED, Kepe V, Ercoli LM, Siddarth P, et al. Localization of neurofibrillary tangles and beta-amyloid plaques in the brains of living patients with Alzheimer disease. Am J Geriatr Psychiatry. 2002;10:24–35.
4. Mathis CA, Wang Y, Holt DP, Huang GF, Debnath ML, Klunk WE. Synthesis and evaluation of 11C-labeled 6-substituted 2-arylbenzothiazoles as amyloid imaging agents. J Med Chem. 2003;46:2740–54. doi:10.1021/jm030026b.
5. Klunk WE, Engler H, Nordberg A, Wang Y, Blomqvist G, Holt DP, et al. Imaging brain amyloid in Alzheimer's disease with Pittsburgh Compound-B. Ann Neurol. 2004;55:306–19. doi:10.1002/ana.20009.
6. Kudo Y, Okamura N, Furumoto S, Tashiro M, Furukawa K, Maruyama M, et al. 2-(2-[2-Dimethylaminothiazol-5-yl]ethenyl)-6- (2-[fluoro]ethoxy)benzoxazole: a novel PET agent for in vivo detection of dense amyloid plaques in Alzheimer's disease patients. J Nucl Med. 2007;48:553–61.
7. Ikonomovic MD, Klunk WE, Abrahamson EE, Mathis CA, Price JC, Tsopelas ND, et al. Post-mortem correlates of in vivo PiB-PET amyloid imaging in a typical case of Alzheimer's disease. Brain. 2008;131:1630–45. doi:10.1093/brain/awn016.
8. Sperling RA, Aisen PS, Beckett LA, Bennett DA, Craft S, Fagan AM, et al. Toward defining the preclinical stages of Alzheimer's disease: recommendations from the National Institute on Aging-Alzheimer's Association workgroups on diagnostic guidelines for Alzheimer's disease. Alzheimers Dement. 2011;7:280–92. doi:10.1016/j.jalz.2011.03.003.
9. Jack Jr CR, Knopman DS, Jagust WJ, Shaw LM, Aisen PS, Weiner MW, et al. Hypothetical model of dynamic biomarkers of the Alzheimer's pathological cascade. Lancet Neurol. 2010;9:119–28. doi:10.1016/S1474-4422(09)70299-6.
10. Pike KE, Savage G, Villemagne VL, Ng S, Moss SA, Maruff P, et al. Beta-amyloid imaging and memory in non-demented individuals: evidence for preclinical Alzheimer's disease. Brain. 2007;130:2837–44. doi:10.1093/brain/awm238.
11. Okamura N, Suemoto T, Furumoto S, Suzuki M, Shimadzu H, Akatsu H, et al. Quinoline and benzimidazole derivatives: candidate probes for in vivo imaging of tau pathology in Alzheimer's disease. J Neurosci. 2005;25:10857–62. doi:10.1523/JNEUROSCI.1738-05.2005.
12. Fodero-Tavoletti MT, Okamura N, Furumoto S, Mulligan RS, Connor AR, McLean CA, et al. 18F-THK523: a novel in vivo tau imaging ligand for Alzheimer's disease. Brain. 2011;134:1089–100. doi:10.1093/Brain/Awr038.
13. Lockhart A, Lamb JR, Osredkar T, Sue LI, Joyce JN, Ye L, et al. PIB is a non-specific imaging marker of amyloid-beta (Abeta) peptide-related cerebral amyloidosis. Brain. 2007;130:2607–15. doi:10.1093/brain/awm191.
14. Burack MA, Hartlein J, Flores HP, Taylor-Reinwald L, Perlmutter JS, Cairns NJ. In vivo amyloid imaging in autopsy-confirmed Parkinson disease with dementia. Neurology. 2010;74:77–84. doi:10.1212/WNL.0b013e3181c7da8e.
15. Clark CM, Schneider JA, Bedell BJ, Beach TG, Bilker WB, Mintun MA, et al. Use of florbetapir-PET for imaging beta-amyloid pathology. JAMA. 2011;305:275–83. doi:10.1001/jama.2010.2008.
16. Wong DF, Moghekar AR, Rigamonti D, Brasic JR, Rousset O, Willis W, et al. An in vivo evaluation of cerebral cortical amyloid with [(18)F]Flutemetamol using positron emission tomography compared with parietal biopsy samples in living normal pressure hydrocephalus patients. Mol Imaging Biol. 2012. doi:10.1007/s11307-012-0583-x.
17. Maeda J, Ji B, Irie T, Tomiyama T, Maruyama M, Okauchi T, et al. Longitudinal, quantitative assessment of amyloid, neuroinflammation, and anti-amyloid treatment in a living mouse model of Alzheimer's disease enabled by positron emission tomography. J Neurosci. 2007;27:10957–68. doi:10.1523/JNEUROSCI.0673-07.2007.

18. Manook A, Yousefi BH, Willuweit A, Platzer S, Reder S, Voss A, et al. Small-animal PET imaging of amyloid-beta plaques with [11C]PiB and its multi-modal validation in an APP/PS1 mouse model of Alzheimer's disease. PLoS One. 2012;7:e31310. doi:10.1371/journal.pone.0031310.
19. Agdeppa ED, Kepe V, Liu J, Flores-Torres S, Satyamurthy N, Petric A, et al. Binding characteristics of radiofluorinated 6-dialkylamino-2-naphthylethylidene derivatives as positron emission tomography imaging probes for beta-amyloid plaques in Alzheimer's disease. J Neurosci. 2001;21:RC189.
20. Gallyas F. Silver staining of Alzheimer's neurofibrillary changes by means of physical development. Acta Morphol Acad Sci Hung. 1971;19:1–8.
21. Barghorn S, Davies P, Mandelkow E. Tau paired helical filaments from Alzheimer's disease brain and assembled in vitro are based on beta-structure in the core domain. Biochemistry. 2004;43:1694–703. doi:10.1021/bi0357006.
22. von Bergen M, Barghorn S, Muller SA, Pickhardt M, Biernat J, Mandelkow EM, et al. The core of tau-paired helical filaments studied by scanning transmission electron microscopy and limited proteolysis. Biochemistry. 2006;45:6446–57. doi:10.1021/bi052530j.
23. Fodero-Tavoletti MT, Mulligan RS, Okamura N, Furumoto S, Rowe CC, Kudo Y, et al. In vitro characterisation of BF227 binding to alpha-synuclein/Lewy bodies. Eur J Pharmacol. 2009;617:54–8. doi:10.1016/j.ejphar.2009.06.042.
24. Thompson PW, Ye L, Morgenstern JL, Sue L, Beach TG, Judd DJ, et al. Interaction of the amyloid imaging tracer FDDNP with hallmark Alzheimer's disease pathologies. J Neurochem. 2009;109:623–30. doi:10.1111/j.1471-4159.2009.05996.x.
25. Braak E, Braak H, Mandelkow EM. A sequence of cytoskeleton changes related to the formation of neurofibrillary tangles and neuropil threads. Acta Neuropathol. 1994;87:554–67.
26. Thal DR, Rub U, Schultz C, Sassin I, Ghebremedhin E, Del Tredici K, et al. Sequence of Abeta-protein deposition in the human medial temporal lobe. J Neuropathol Exp Neurol. 2000;59:733–48.
27. Villemagne VL, Furumoto S, Fodero-Tavoletti M, Harada R, Mulligan RS, Kudo Y, et al. The challenges of tau imaging. Future Neurol. 2012;7:409–21. doi:10.2217/fnl.12.34.
28. Fodero-Tavoletti MT, Smith DP, McLean CA, Adlard PA, Barnham KJ, Foster LE, et al. In vitro characterization of Pittsburgh compound-B binding to Lewy bodies. J Neurosci. 2007;27:10365–71. doi:10.1523/JNEUROSCI.0630-07.2007.
29. Klunk WE, Lopresti BJ, Ikonomovic MD, Lefterov IM, Koldamova RP, Abrahamson EE, et al. Binding of the positron emission tomography tracer Pittsburgh compound-B reflects the amount of amyloid-beta in Alzheimer's disease brain but not in transgenic mouse brain. J Neurosci. 2005;25:10598–606. doi:10.1523/JNEUROSCI.2990-05.2005.
30. Klunk WE, Wang Y, Huang GF, Debnath ML, Holt DP, Shao L, et al. The binding of 2-(4'-methylaminophenyl)benzothiazole to post-mortem brain homogenates is dominated by the amyloid component. J Neurosci. 2003;23:2086–92.
31. Shin J, Lee SY, Kim SH, Kim YB, Cho SJ. Multitracer PET imaging of amyloid plaques and neurofibrillary tangles in Alzheimer's disease. Neuroimage. 2008;43:236–44. doi:10.1016/j.neuroimage.2008.07.022.

MOLECULAR IMAGING AND BIOLOGY

Mol Imaging Biol (2013) 15:497–506
DOI: 10.1007/s11307-012-0608-5

Published Online: 30 January 2013

World Molecular Imaging Society

RESEARCH ARTICLE

A ^{18}F-Labeled BF-227 Derivative as a Potential Radioligand for Imaging Dense Amyloid Plaques by Positron Emission Tomography

Shozo Furumoto,[1,2] Nobuyuki Okamura,[1] Katsutoshi Furukawa,[3] Manabu Tashiro,[4] Yoichi Ishikawa,[2] Kentaro Sugi,[1] Naoki Tomita,[3] Masaaki Waragai,[3] Ryuichi Harada,[1] Tetsuro Tago,[2] Ren Iwata,[2] Kazuhiko Yanai,[1] Hiroyuki Arai,[3] Yukitsuka Kudo[5]

[1]*Department of Pharmacology, Tohoku University School of Medicine, 2-1 Seiryo-machi, Aoba-ku, Sendai 980-8575, Japan*
[2]*Division of Radiopharmaceutical Chemistry, Cyclotron and Radioisotope Center, Tohoku University, Sendai, Japan*
[3]*Department of Geriatrics and Gerontology, Division of Brain Sciences, Institute of Development, Aging and Cancer, Tohoku University, Sendai, Japan*
[4]*Division of Cyclotron Nuclear Medicine, Cyclotron and Radioisotope Center, Tohoku University, Sendai, Japan*
[5]*Clinical Research, Innovation and Education Center, Tohoku University Hospital, Sendai, Japan*

Abstract

Purpose: The aims of this study were to evaluate the binding and pharmacokinetics of novel ^{18}F-labeled ethenyl-benzoxazole derivatives (i.e., [^{18}F] fluorinated amyloid imaging compound of Tohoku university ([^{18}F]FACT)) as amyloid positron emission tomography (PET) tracers and to assess [^{18}F]FACT efficacy in imaging of Alzheimer's disease (AD).

Procedures: Binding assay was conducted using synthetic amyloid-β (Aβ) fibrils, fluorescence microscopy, and autoradiogram in three postmortem AD brains. Pharmacokinetics of [^{18}F]FACT was assessed using 12 Crj:CD-1 (ICR) mice. *In vivo* binding ability with brain amyloid was investigated using amyloid precursor protein (APP) transgenic mouse. Clinical PET scanning using [^{18}F]FACT was performed in ten healthy controls and ten mild cognitive impairment and ten AD patients.

Results: [^{18}F]FACT showed high binding affinity for synthetic Aβ fibrils, preferential binding to dense cored plaques in brain sections, and excellent brain uptake and rapid clearance in mice. Injection in APP mice resulted in specific *in vivo* labeling of amyloid deposits in the brain. PET scans of AD patients showed significantly higher [^{18}F]FACT uptake in the neocortex compared to controls ($P<0.05$, Kruskal–Wallis test).

Conclusion: [^{18}F]FACT is a promising agent for imaging dense Aβ plaques in AD.

Key words: Alzheimer's disease, Amyloid, Early diagnosis, Positron emission tomography

Introduction

Alzheimer's disease (AD) is an age-dependent and irreversible neurodegenerative disorder leading to deterioration of memory and cognitive function. Although the exact mechanisms underlying pathogenesis of AD are not fully understood, formation of brain amyloid plaques through aggregation and deposition of amyloid-β protein (Aβ) is considered to be the initial pathogenic event that may precede the appearance of clinical AD symptoms by decades. Recently, new criteria for diagnosing AD were proposed by the National Institute on Aging—Alzheimer's Association workgroups [1]. The new diagnostic criteria include the use of biomarkers for amyloid deposition to aid

Correspondence to: Nobuyuki Okamura; *e-mail:* nookamura@med.tohoku.ac.jp

in diagnosis of AD. Thus, *in vivo* detection of amyloid depositions with positron emission tomography (PET) has received much attention as a potential technology for early or presymptomatic diagnosis of AD. For this purpose, a number of radiotracers for Aβ aggregates have been synthesized and evaluated as candidates for PET amyloid imaging agents, and some of these are undergoing clinical investigation [2–4].

Among them, *N*-methyl-[^{11}C]-2-(4′-methylaminophenyl)-6-hydroxybenzothiazole ([^{11}C]Pittsburgh compound B, [^{11}C]PiB) is currently the most widely used in clinical research [5]. Labeling of PET tracers with ^{18}F ($T_{1/2}$= 109.8 min) allows time for their delivery to numerous PET centers and contributes to spreading their use. Several ^{18}F-labeled amyloid PET tracers, including [^{18}F]flutemetamol, [^{18}F]florbetaben, [^{18}F]florbetapir, and [^{18}F]AZD4694, have been developed, and to date, [^{18}F]florbetapir has become commercially available [6–9]. An increasing number of PET studies in humans have clearly demonstrated that amyloid PET is a potentially useful technique to visualize and quantify the distribution of Aβ plaques of AD patients [5]. In addition, a proportion of elderly normal subjects present with [^{11}C]PiB retention in the neocortex [10–12], suggesting that amyloid PET is potentially useful for presymptomatic detection of Aβ pathology. Although neocortical PiB retention is considered as a high risk for future cognitive decline, not all PiB-positive normal individuals are destined to develop dementia. Some additional biomarkers are thus necessary for accurate prediction of future conversion to dementia. According to previous histopathological study, progression to dementia is associated with a shift from non-fibrillar to fibrillar amyloid deposits in the brain [13]. Thus, selective detection of dense fibrillar amyloid might be advantageous for predicting progression to dementia.

Previously, we had succeeded in developing a unique scaffold of a radioligand, [^{11}C]2-(2-[2-dimethylaminothiazol-5-yl]ethenyl)-6-(2-[fluoro]ethoxy)benzoxazole ([^{11}C]BF-227), as an amyloid imaging probe [3, 14]. Our previous study demonstrated that Aβ deposits in AD patients can be clearly detected by [^{11}C]BF-227 PET [15]. Neocortical [^{11}C]BF-227 retention was further observed in subjects with mild cognitive impairment (MCI) [16]. Using [^{11}C]BF-227 PET, we achieved a sensitivity of 100 % and a specificity of 71.4 % in distinguishing MCI converters to AD from MCI non-converters [17], suggesting the usefulness of this radiotracer for accurate prediction of future progression to dementia. To further take advantage of this imaging potential, especially in a large clinical study, we anticipated that a ^{18}F-labeled derivative of BF-227 would be valuable due to the longer half-life of ^{18}F compared with ^{11}C.

In this study, we performed a biological evaluation of a series of ^{18}F-labeled 2-ethenyl-benzoxazole derivatives (Fig. 1) to select a candidate for clinical application. The one selected, [^{18}F]Fluorinated Amyloid Imaging Compound of Tohoku University ([^{18}F]FACT), was further evaluated for its binding characteristics with Aβ fibrils and plaques and then for its clinical utility as a probe for imaging amyloid in AD.

Methods

Radiosynthesis of ^{18}F-Labeled 2-Ethenyl-Benzoxazole Derivatives

The chemical structures of the 2-ethenyl-benzoxazole derivatives are summarized in Fig. 1. The compounds and their precursors for ^{18}F-labeling were synthesized according to the method described previously [18]. ^{18}F-labeled compounds were prepared according to the following method. The aqueous $^{18}F^-$ contained in K_2CO_3 solution (1.27 to 3.28 GBq) and Kryptofix 2.2.2 were put into a brown vial, and then the water was azeotropically removed with acetonitrile by heating at 110 °C and He-gas flow. After drying, the activated [^{18}F]KF/Kryptofix 2.2.2. was reacted with a tosylate precursor in dimethyl sulfoxide (DMSO) at 110 °C for 10 min, followed by addition of water to quench. The product was extracted by solid-phase extraction with Sep-Pak ^{t}C18 cartridge (Waters) and then eluted with ethanol. The ^{18}F-labeled compound was separated from the eluent by semi-preparative reversed-phase high-performance liquid chromatography (RP-HPLC), isolated from the collected fraction by solid-phase extraction with Sep-Pak ^{t}C18

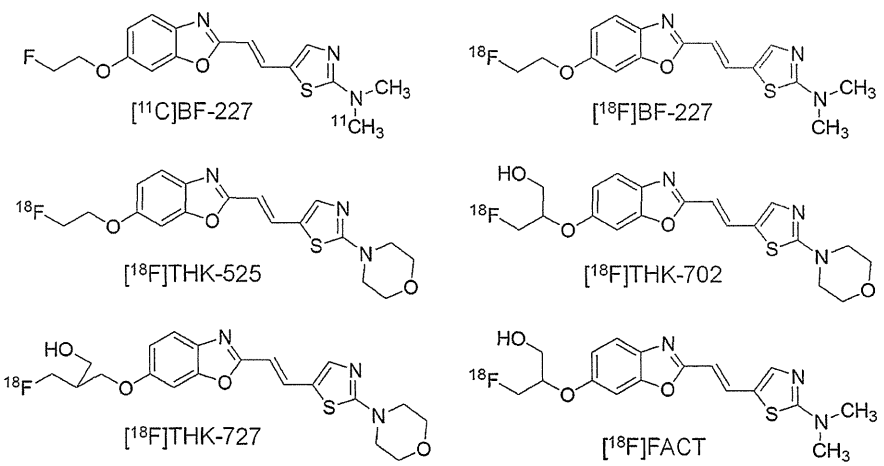

Fig. 1. Chemical structures of [^{11}C]BF-227 and its ^{18}F-labeled 2-ethenyl benzoxazole derivatives.

cartridge, and finally dissolved in DMSO or saline with polysorbate-80 (<0.1 %) for biological evaluation.

[^{11}C]BF-227 was synthesized from the precursor by *N*-methylation with [^{11}C]methyl triflate in DMSO and separated from the crude mixture by semi-preparative RP-HPLC, as described previously [15]. The purified [^{18}F]FACT and [^{11}C]BF-227 were solubilized in isotonic saline containing 1 % polysorbate-80 and 5 % ascorbic acid and then filter-sterilized with 0.22 μm Millipore filter for clinical use.

Fluorescent Staining

Postmortem brain tissue from a 69-year-old man with autopsy-confirmed AD was obtained from Fukushimura Hospital (Toyohashi, Japan). Experiments were performed under the regulations of the hospital ethics committee. Serial sections (6 μm) taken from paraffin-embedded blocks of the temporal cortex were prepared in xylene and ethanol. Before staining with test compounds, quenching of autofluorescence was performed. The quenched tissue section was immersed in 100 μM of test compounds containing 50 % ethanol for 10 min. The stained section was then dipped briefly into water before coverslipping with FluorSave Reagent (Calbiochem, La Jolla, CA, USA) and examination using an Eclipse E800 microscope (Nikon, Tokyo, Japan) equipped with a V-2A filter set (excitation 380 to 420 nm, dichroic mirror 430 nm, long pass filter 450 nm). An adjacent section was immunostained using 4G8 (Signet, Dedham, MA, USA), a monoclonal antibody against Aβ. After pretreatment with 90 % formic acid for 5 min, sections were immersed in blocking solution for 30 min and then incubated for 60 min at 37 °C with 4G8 at a dilution of 1:100. After incubation, sections were processed with biotinylated anti-mouse IgG (Wako) for 60 min, followed by Texas Red-conjugated streptavidin (Vector Laboratories, Burlingame, CA, USA).

In Vitro Autoradiography

A temporal brain section from a 76-year-old female AD patient was incubated with 1.85 MBq/ml of [^{18}F]FACT at room temperature for 20 min and then washed briefly with water and 70 % ethanol. After drying, the labeled section was exposed to a BAS-III imaging plate (Fuji Film, Tokyo, Japan) for 120 min. Autoradiograms were obtained using a BAS-5000 phosphor imaging instrument (Fuji Film, Tokyo, Japan). Neighboring sections were immunostained using 4G8 anti-Aβ monoclonal antibody. After incubation with 4G8, sections were processed by the avidin–biotin method using a Pathostain ABC-POD(M) Kit (Wako, Osaka, Japan) and diaminobenzidine tetrahydrochloride.

In Vitro Binding Study

Amyloid β_{1-40} (Peptide Institute, Inc., Japan) was dissolved in 50 mM potassium phosphate buffer (pH 7.4) to a final concentration of 20 μM. To prepare amyloid fibrils, the solution was incubated at 37 °C for 4 days at 85 rpm and then sonicated to obtain a uniform suspension. The fibril solution was diluted to 2 μM with phosphate-buffered saline (PBS) containing 0.1 % bovine serum albumin (BSA). For saturation binding assay, 100 μl of the fibril solution was mixed with [^{18}F]FACT solution (0.2 to 800 nM, PBS containing 0.1 % BSA and 2 % DMSO, 100 μl) in a 96-well plate. Non-specific binding was defined in the presence of 2 μM FACT in the final solution. The mixture was incubated for 40 min at room temperature and then was passed through the glass filter plate under vacuum with MultiScreen HTS Vacuum Manifold (Millipore Corp., USA), followed by washing with PBS containing 0.1 % BSA twice. Radioactivity of the filter was counted with an automatic gamma counter. The binding data were analyzed with curve-fitting software that calculates the K_d and B_{max} using non-linear regression (GraphPad Prism Version 5.0, GraphPad Software, San Diego, CA, USA).

Biodistribution Study in Normal Mice

The experimental protocols were reviewed by the Committee on the Ethics of Animal Experiments at Tohoku University School of Medicine and performed in accordance with the Guidelines for Animal Experiments issued by the Tohoku University School of Medicine. Male Crj:CD-1 (ICR) mice (6 weeks old, 25 to 30 g, n=12) were injected in a lateral tail vein with ^{18}F-labeled test compounds (370 to 740 kBq) contained in isotonic saline (0.2 ml). The mice were sacrificed by cervical dislocation following heart puncture to obtain blood samples at 2, 30, and 60 min postinjection (n=4 at each time point). Tissues of interest were excised and weighed, and the radioactivity was counted in an automatic gamma-counter. Radioactivity uptake data are expressed as percent of injected dose per gram of tissue (%ID/g).

Autoradiography of Aβ Deposits in Living Transgenic Mice

An amyloid precursor protein (APP) transgenic (Tg) mouse (female, 31 months old) and a wild-type littermate (female, 31 months old) were injected with [^{18}F]FACT (37 MBq) *via* tail vein. The mice were sacrificed by cervical dislocation at 2 h postinjection, and the brains were rapidly excised and frozen in liquid nitrogen. Frozen sections of 20 μm thick were prepared from the brains for *ex vivo* autoradiography. Autoradiograms were obtained in the same manner described above. The sections used for autoradiography were then subjected to fluorescent staining with thioflavin-S according to the previously described method [19].

Clinical PET Study Using [^{18}F]FACT

Ten patients with amnestic MCI, ten patients with AD, and ten normal age-matched controls participated in the clinical PET study using [^{18}F]FACT. Please refer to Table 1 for characteristics of participants. [^{11}C]BF-227 PET scan was additionally performed in two patients with AD (70-year-old woman (MMSE score 17) and 79-year-old man (MMSE score 20)) and 1 normal control subject (60-year-old man (MMSE score 30)). The average time interval between [^{18}F]FACT and [^{11}C]BF-227 PET scans was 12±6 months. Diagnosis of probable AD was based on criteria from the National Institute of Neurological and Communicative Disorders and Stroke and the Alzheimer's Disease Related Disorders Association [20]. The diagnosis of amnestic MCI was made according to published criteria described previously [21]. The control subjects were

Table 1. Subject and patient demographics in [^{18}F]FACT PET comparisons

	NC	MCI	AD
N	10	10	10
Gender (F/M)	4/6	7/3	7/3
Age (years)	69.8±8.8 (60–89)	74.2±8.8 (57–89)	74.5±4.6 (66–81)
MMSE score	29.9±0.3 (29–30)	26.4±1.1 (24–28)	19.8±3.0 (15–24)

recruited from volunteers who were taking no centrally acting medications, had no cognitive impairment, and had no cerebrovascular lesions, including asymptomatic cerebral infarction on T2-weighted studies, identified *via* MRI. All volunteers were screened using a questionnaire and medical history, and those with medical conditions potentially affecting the central nervous system were excluded. The Committee on Clinical Investigation at Tohoku University School of Medicine and the Advisory Committee on Radioactive Substances at Tohoku University approved the study protocol. After complete description of the study to the patients and subjects, written informed consent was obtained.

Image Acquisition Protocols

[^{18}F]FACT-PET and [^{11}C]BF-227-PET study was performed using a SET-2400W PET scanner (Shimadzu, Kyoto, Japan). After intravenous injection of 111–185 MBq of [^{18}F]FACT or 211–366 MBq of [^{11}C]BF-227, dynamic PET images were obtained for 60 min (23 sequential scans; 5 scans×30 s, 5 scans×60 s, 5 scans×150 s, and 8 scans×300 s) with the subject's eyes closed. SUV summation images at 0–10, 10–20, 20–30, 30–40, 40–50, and 50–60 min postinjection were created for the analysis of tracer uptake. T1-weighted MR images were obtained using a SIGNA 1.5 T machine (General Electric, Milwaukee, WI, USA).

Image Analysis

Firstly, standardized uptake value (SUV) images of [^{18}F]FACT and [^{11}C]BF-227 were obtained by normalizing tissue radioactivity concentration by injected dose and body weight. Subsequently, individual MR images were anatomically coregistered into individual PET images using Statistical Parametric Mapping software (SPM5: Welcome Department, UK). Regions of interest (ROIs) were placed on individual axial MR images in the cerebellar hemisphere, frontal cortex [Brodmann's areas (BA) 8, 9, 10, 44, 45, 46, and 47], lateral temporal cortex (BA 21, 22, 37, and 38), parietal cortex (BA 39 and 40), occipital cortex (BA 17), anterior cingulate cortex, posterior cingulate cortex, medial temporal cortex (BA 27, 28, 34, and 35), striatum, pons, and subcortical white matter, as described previously [15]. The ROI information was then copied onto dynamic PET SUV images, and regional SUVs were sampled using PMOD software (PMOD Technologies, Ltd., Zurich, Switzerland). The ratio of regional SUV to cerebellar SUV (SUVR) was calculated as an index of tracer retention. Averaged SUVR in the frontal, temporal, parietal, and posterior cingulate cortices was considered representative of tracer retention in the neocortex (neocortical SUVR). The inter-rater reliability for the ROI measurement was tested between two raters (N.O. and K.S.) in seven subjects and patients. The intra-class correlation coefficient was 0.95.

Statistical Analysis

For statistical comparison in the three groups, we applied the Kruskal–Wallis test followed by Dunn's multiple comparison test. Differences of time activity curves (TACs) in [^{18}F]FACT PET were also evaluated by repeated measures ANOVA followed by the Bonferroni–Dunn post hoc test. For statistical comparisons of PET measurements in control and AD groups, we used the Mann–Whitney *U* test. Effect size coefficients (Cohen's *d*) were also calculated for the evaluation of group differences in PET measurements. Statistical significance for each analysis was defined as $P<0.05$. Correlations between [^{18}F]FACT and [^{11}C]BF-227 SUVR in the frontal, temporal, parietal, and occipital cortices of three subjects (two AD and one normal control) were determined using Pearson's correlations. A linear model was applied to the data to obtain a correlation coefficient and *p* value. These analyses were performed using GraphPad Prism5 software (GraphPad, San Diego, CA, USA).

Results

Radiosynthesis

^{18}F-labeled 2-ethenyl-benzoxazole derivatives (Fig. 1) were obtained in yields of 32 % on average (21 to 44 %, decay-corrected) with radiochemical purity greater than 99 % after HPLC purification. The specific activities ranged 70 to 180 GBq/μmol, corrected at the end of synthesis.

In Vitro Binding to Aβ Plaques in AD Brain Sections

Binding ability of 2-ethenyl-benzoxazole derivatives to Aβ plaques was examined using AD brain sections from a 69-year-old man with autopsy-confirmed AD. As shown in Fig. 2a, c, dense cored plaques (arrowheads) were clearly stained with FACT. In particular, Aβ plaque cores were brightly stained with this compound. The fluorescent staining pattern of FACT correlated well with Aβ immunostaining (Fig. 2b) and thioflavin-S staining (Fig. 2d) in adjacent sections. Other compounds produced similar results in the histopathological staining of AD brain sections from a 69-year-old man with autopsy-confirmed AD.

In vitro autoradiography at tracer dose indicated [^{18}F]FACT binding to dense Aβ deposits (arrowheads) in AD temporal brain sections from a 76-year-old female AD patient (Fig. 2e–h). Tracer signals were additionally detected

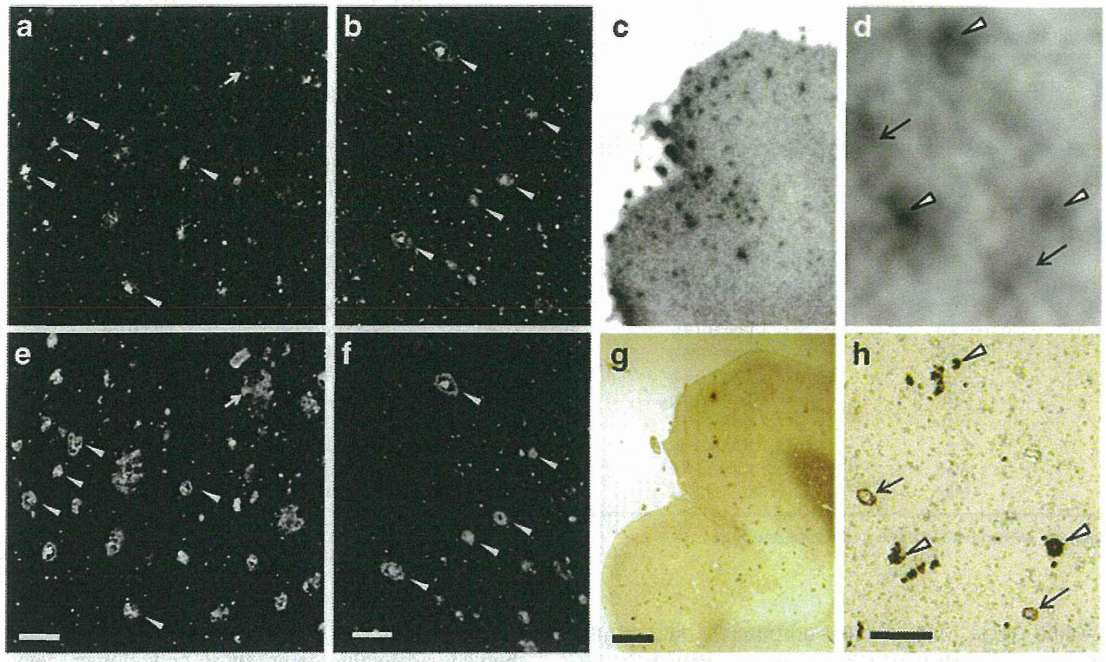

Fig. 2. **a–d** Fluorescence microscopy images of AD brain sections from a 69-year-old man with autopsy-confirmed AD stained with FACT (**a**, **c**), anti-Aβ (4 G8) antibody (**b**), and thioflavin-S (**d**). *Arrowheads* delineate dense cored plaques, respectively. **e–h** Autoradiogram of AD brain section from a 76-year-old female AD patient with [^{18}F]FACT (**e**, **g**) and images of the adjacent section immunostained with anti-Aβ (4 G8) antibody (**f**, **h**). *Arrows* and *arrowheads* delineate congophilic amyloid angiopathy and dense cored plaques, respectively. *Bars* 100 μm (**a–d**), 2 mm (**e–f**), 200 μm (**g–h**).

in congophilic amyloid angiopathy (arrows). These results indicated that FACT and its derivatives had an ability to detect pathological dense Aβ deposits in AD brain tissue.

Binding Affinity to Synthetic Aβ Fibrils

Binding properties of [^{18}F]FACT with Aβ fibrils were investigated by *in vitro* binding assay. Scatchard analysis of FACT binding to Aβ fibrils showed two classes of binding sites: a high-affinity site (K_d=9.4 nM; B_{max}= 0.16 pmol/nmol of Aβ) and a low-affinity site (K_d= 263 nM; B_{max}=1.52 pmol/nmol of Aβ).

Biodistribution Study in Normal Mice

Two important properties of an amyloid imaging probe are rapid brain uptake and rapid clearance from the normal brain without non-specific binding. These properties of the ^{18}F-labeled 2-ethenyl-benzoxazole derivatives were evaluated by biodistribution studies in 12 normal mice (n=4 at each time point). The radioactivity uptake in the blood, brain, liver, kidney, and bone is summarized in Table 2. Regarding brain uptake, all of the ^{18}F-labeled derivatives showed rapid and sufficient brain uptake (4 to 6 %ID/g at 2 min) and smooth washout after that. However, the brain uptake at 60 min varied from 0.28 to 1.68 %ID/g, suggesting a different clearance property in normal brain. Among the derivatives, [^{18}F]FACT indicated the highest ratio of brain uptakes at 2 min to that at 60 min (4.64/0.28=16.6). Additionally, mice injected with [^{18}F]FACT exhibited no increase of the radioactivity uptake in bone with time, unlike with [^{18}F]BF-227, suggesting that [^{18}F] FACT has good stability in regard to metabolic defluorination *in vivo*. Thus, we selected [^{18}F]FACT as the candidate for the clinical comparisons.

Autoradiography of Aβ Deposits in Living Transgenic Mouse

In vivo binding ability of [^{18}F]FACT with amyloid plaques was evaluated in the APP-Tg mouse. Autoradiographic images of the APP-Tg mouse brain post-intravenous injection of [^{18}F]FACT displayed high uptake of the labeling compound in the cortex and hippocampus (Fig. 3a). In contrast, no notable binding was observed in the brain of wild-type mouse (Fig. 3b). These [^{18}F]FACT binding results in APP-Tg mouse brain corresponded closely with those of *in vitro* thioflavin-S staining in the same brain sections (Fig. 3c, d). These results warranted further clinical investigation of [^{18}F]FACT PET in AD patients.

Clinical PET Study Using [^{18}F]FACT

Demographic data for the participants are summarized in Table 1. No statistical difference in age was observed among the three groups. MCI and AD patients had significantly lower mean MMSE scores than normal controls (P<0.05,

Table 2. Biodistribution of ^{18}F-labeled compounds in mice

Tracers	Time (min)	Radioactivity uptakes (%ID/g)				
		Blood	Brain	Liver	Kidney	Bone
[^{18}F]BF-227	2	2.93±0.08	6.05±0.45	7.97±1.59	9.63±0.89	1.59±0.27
	30	2.14±0.17	1.91±0.05	5.75±0.42	3.04±0.15	4.38±1.24
	60	2.09±0.15	1.67±0.14	5.48±0.23	2.42±0.20	7.04±0.75
[^{18}F]THK-525	2	2.82±0.38	4.73±1.32	5.93±1.40	7.72±2.44	1.77±0.87
	30	2.20±0.24	2.05±0.16	3.55±0.60	2.32±0.18	6.74±2.20
	60	1.91±0.29	1.68±0.15	2.47±0.23	1.48±0.14	9.65±0.89
[^{18}F]THK-702	2	3.34±0.13	4.15±0.28	7.53±0.50	13.6±0.88	1.95±0.34
	30	1.06±0.19	0.53±0.03	4.55±0.39	1.58±0.64	0.92±0.11
	60	0.67±0.08	0.35±0.04	3.65±0.72	0.65±0.09	1.16±0.70
[^{18}F]THK-727	2	2.94±0.33	4.06±0.26	9.89±4.16	11.4±1.35	2.08±0.39
	30	1.52±0.10	1.04±0.08	6.68±1.22	2.47±0.36	6.61±0.79
	60	0.66±0.10	0.69±0.02	4.04±1.87	0.98±0.14	9.33±1.34
[^{18}F]FACT	2	3.65±0.66	4.64±0.55	9.38±0.43	10.2±1.05	1.84±0.18
	30	1.19±0.49	0.53±0.11	11.3±1.32	4.17±0.44	0.88±0.07
	60	0.64±0.13	0.28±0.04	14.1±0.55	3.25±0.27	1.38±0.46

Data are expressed as mean±SD (n=4 at each time point)

Kruskal–Wallis test). AD patients additionally had significantly lower mean MMSE scores than those with MCI ($P<$ 0.05, Kruskal–Wallis test). No toxic events were observed in the current clinical trial. The SUV-TACs from [^{18}F]FACT-PET in AD patients and normal control subjects are shown in Fig. 4. Both groups showed rapid entry of [^{18}F]FACT into the neocortex and cerebellum. In the AD patients, the temporal cortex, known to contain high concentrations of fibrillar amyloid plaques in AD, showed retention of [^{18}F] FACT during the later time points compared with the cerebellum (Fig. 4a). In contrast, TACs in the temporal cortex and the cerebellum were nearly identical in normal subjects (Fig. 4b). The subcortical white matter regions showed relatively lower entry and slower clearance than gray matter areas, but no difference in TACs between AD patients and normal controls.

SUVR in the lateral temporal cortex of AD patients was significantly higher over 10 min postinjection of [^{18}F]FACT than those of normal controls ($p<0.05$, Mann–Whitney U test) and reached maximum value at 30 to 40 min postinjection (Fig. 4c). Effect size between AD and normal controls showed the highest value at 30 to 40 min postinjection of [^{18}F]FACT (Table 3). The ratio of SUVR in AD to SUVR in normal controls became constant after

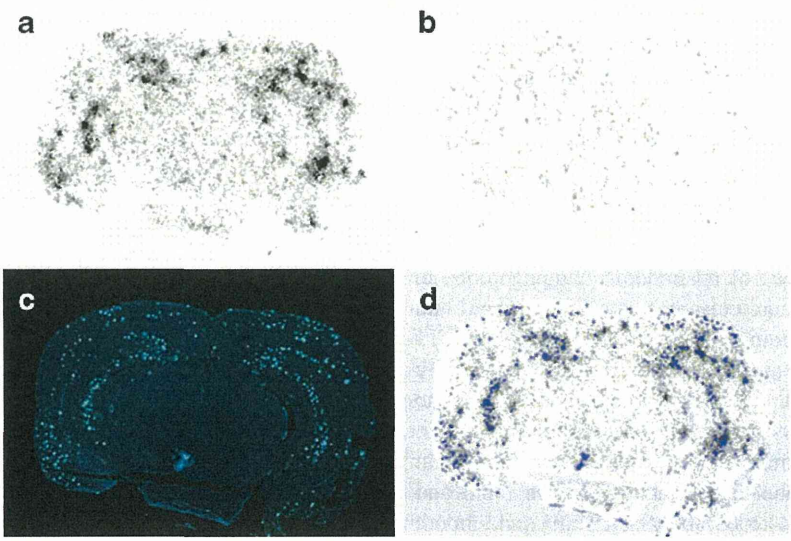

Fig. 3. *Ex vivo* autoradiograms of brain sections from APP transgenic (Tg) mouse (**a**) and wild type mouse (**b**). The brains were excised at 2 h after intravenous injection of [^{18}F]FACT. Aβ plaques in APP-Tg mouse brain were clearly stained with thioflavin-S (**c**). A merged image of **a** and **c** is shown in **d**.

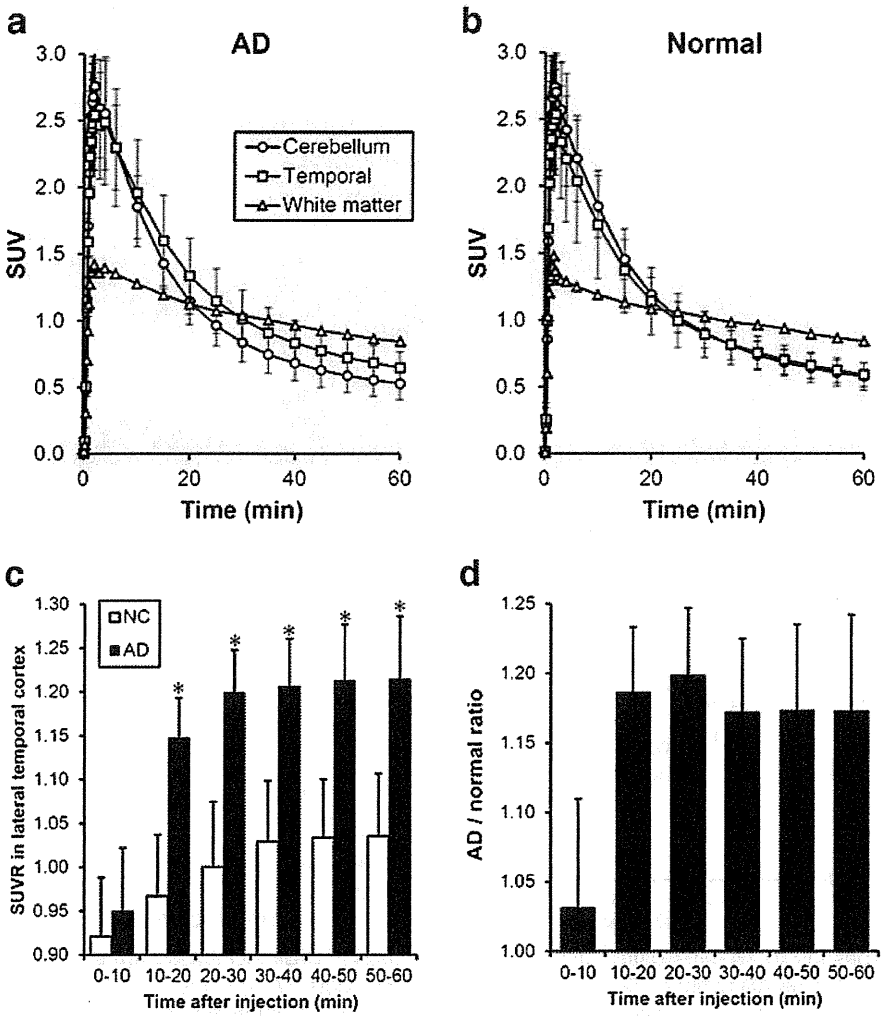

Fig. 4. Time activity data for [^{18}F]FACT PET in humans. Time activity curves of [^{18}F]FACT in ten AD patients (**a**) and ten normal controls (**b**) are shown. Each point represents the mean±standard deviations of data. Time course of [^{18}F]FACT SUVR in the lateral temporal cortex (**c**) and AD *vs* normal ratio of SUVR in the lateral temporal cortex (**d**) are also shown. *$P<0.05$ by the Mann–Whitney *U* test.

30 min (Fig. 4d). Based on these results, we selected summed dynamic images from 30 to 40 min for the ROI analysis of PET data.

SUVR images of [^{18}F]FACT for a normal control subject (a 60-year-old man, MMSE score 30) and an AD patient (70-year-old woman, MMSE score 17) are shown in Fig. 5a. Cortical retention of [^{18}F]FACT at 30 to 40 min postinjection was evident in the AD patient, as contrasted with the images of the normal control subject. This pattern of distribution was consistent with the distribution of [^{11}C]BF-227 at 30 to 40 min postinjection in the same subject and patient pair (Fig. 5a). The SUV-TACs from [^{18}F]FACT-PET were compared with those from [^{11}C]BF227-PET in the same AD patient (70-year-old woman, MMSE score 17). As shown in Fig. 5b, [^{18}F]FACT showed faster washout from both temporal cortex and cerebellum than [^{11}C]BF-227. The regional SUVR of [^{18}F]FACT at 30 to 40 min postinjection was compared with that of [^{11}C]BF-227 at the same time frame. SUVR values in the frontal, temporal, parietal, and occipital cortices of three subjects (two AD and one normal control) were used for this analysis. As shown in Fig. 5c, regional SUVR of [^{18}F]FACT were significantly correlated with that of [^{11}C]BF-227 (Pearson's r= 0.931, $P<0.001$) in these three subjects.

In the quantitative comparison of regional SUVR 30 to 40 min post-administration, the values for the frontal, lateral

Table 3. Time course of lateral temporal [^{18}F]FACT SUVR and effect size measures in ten normal controls and ten AD patients

Time (min)	Normal control	AD	Cohen's *d*
30–40	1.07±0.06	1.22±0.05*	2.67
40–50	1.08±0.06	1.23±0.06*	2.37
50–60	1.09±0.06	1.23±0.06*	2.34

*$P<0.05$ by the Mann–Whitney *U* test

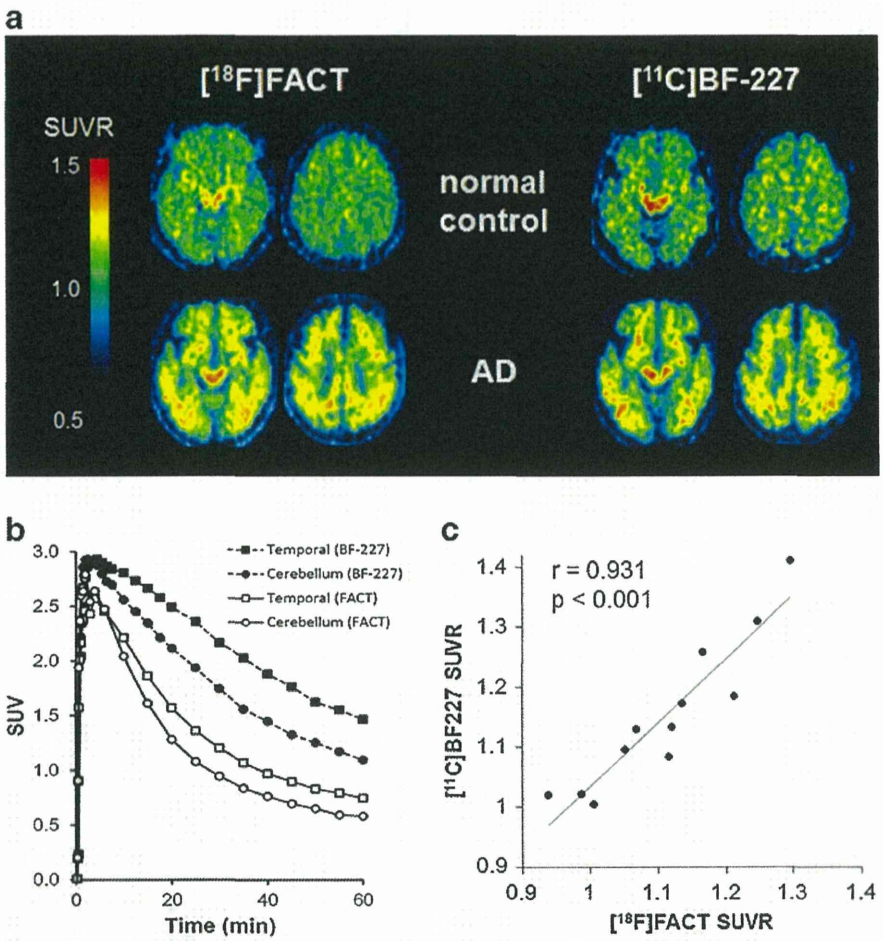

Fig. 5. **a** SUVR images (30 to 40 min postinjection) of [^{18}F]FACT and [^{11}C]BF-227 for a normal control subject (60-year-old man, MMSE score 30) and an AD patient (70-year-old woman, MMSE score 17). **b** Time activity curves of [^{18}F]FACT and [^{11}C]BF-227 in an AD patient (70-year-old woman, MMSE score 17). **c** Significant correlation between regional SUVR of [^{18}F]FACT and [^{11}C]BF-227 in two AD (70-year-old woman (MMSE score 17) and 79-year-old man (MMSE score 20)) and one normal control (60-year-old man, MMSE score 30) subjects (Pearson's r=0.931, P<0.001).

temporal, parietal, occipital, and anterior and posterior cingulate cortices were significantly greater in AD patients than in the normal controls (Table 4). In addition, the SUVRs for the lateral temporal, parietal, occipital, and anterior and posterior cingulate cortices were significantly greater in AD patients than in those with MCI. As shown in Fig. 6, averaged neocortical SUVR was also significantly greater in AD patients than in normal control subjects and MCI (P<0.05, Kruskal–Wallis test). MCI patients additionally showed significantly greater SUVR in the lateral temporal and frontal cortices than normal subjects, but not significant in other brain regions (P<0.05, Kruskal–Wallis

Table 4. Regional SUVR (30 to 40 min postinjection) and effect size measures of [^{18}F]FACT in ten normal controls and ten MCI and ten AD patients

	Normal control	MCI	AD	Cohen's d NC *vs.* AD
Frontal	1.00±0.10	1.09±0.04*	1.15±0.06*	1.82
Lateral temporal	1.05±0.08	1.13±0.06*	1.21±0.05*,**	2.40
Parietal	1.07±0.07	1.13±0.07	1.21±0.08*,**	1.86
Occipital	1.09±0.08	1.07±0.06	1.17±0.05*,**	1.20
Anterior cingulate	1.08±0.07	1.12±0.08	1.21±0.08*,**	1.73
Posterior cingulate	1.15±0.07	1.17±0.06	1.30±0.07*,**	2.14
Medial temporal	1.10±0.05	1.13±0.04	1.15±0.09	0.69
Striatum	1.31±0.11	1.30±0.06	1.35±0.12	0.35
Pons	1.55±0.15	1.57±0.10	1.54±0.09	0.08
White matter	1.50±0.21	1.47±0.11	1.52±0.13	0.12
Neocortex	1.04±0.07	1.12±0.05	1.19±0.05*,**	2.47

*P<0.05 (vs normal control group) and **P<0.05 (vs MCI group) by the Kruskal–Wallis test followed by Dunn's multiple comparison test

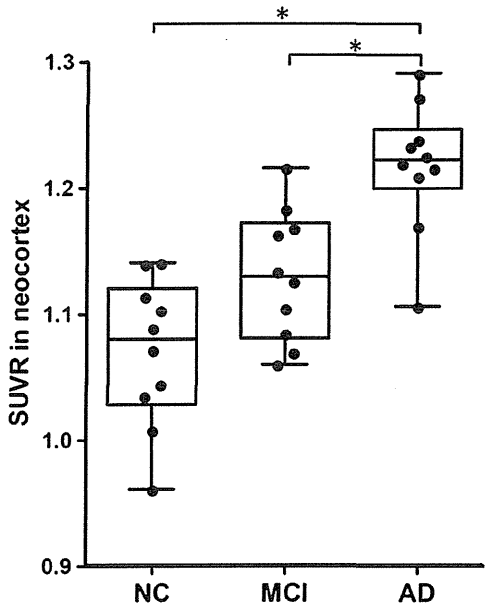

Fig. 6. Comparison of neocortical SUVR of [^{18}F]FACT among ten aged normal controls (NC) and ten mild cognitive impairment (MCI) and ten AD patients. The neocortical SUVRs are represented in a *box* and *whisker plot*. *P<0.05 by the Kruskal–Wallis test followed by Dunn's multiple comparison test.

test). The SUVR in the medial temporal cortex and striatum showed the tendency to be greater in AD patients, but this was not significant. The SUVR in the pons and white matter was nearly identical in AD, MCI, and normal subjects. Effect size value between AD and aged normal subjects was the highest in the lateral temporal cortex (2.40), followed by the posterior cingulate (2.14), parietal (1.86), frontal (1.82), and anterior cingulate (1.73) and occipital (1.20) cortices (Table 4).

Discussion

The current study demonstrated that [^{18}F]FACT PET can be used to detect AD pathology in AD patients and to confirm its absence in cognitively unimpaired elderly people. We previously reported the ability of [^{11}C]BF-227-PET to detect Aβ deposits in the brains of AD patients [15]. The current study has further demonstrated the binding preference of [^{18}F]FACT to dense Aβ plaques in the brains of AD patients. A similar pattern of tracer distribution was observed between [^{18}F]FACT and [^{11}C]BF-227 in AD patients, indicating that [^{18}F]FACT-PET could be substituted for [^{11}C]BF-227-PET for noninvasive detection of dense Aβ deposits in the brain of AD patients. The correlation of [^{18}F]FACT uptake *in vivo* and brain pathology at autopsy should be examined in the future. Our previous studies demonstrated the unique ability of [^{11}C]BF-227 to detect certain forms of prion and α-synuclein protein deposits [22, 23]. Further study will be required to validate the practical usefulness of [^{18}F]FACT-PET for noninvasive detection of these protein deposits.

When a neocortical [^{18}F]FACT SUVR of 1.145 (1.5 SD above control mean) was used as a cutoff, [^{18}F]FACT-PET scan achieved a sensitivity of 90 % (nine of ten) and a specificity of 100 % (ten of ten) in the discrimination between AD patients and normal subjects. In one exception, a 76-year-old female AD patient, MMSE score 24, showed no remarkable retention of [^{18}F]FACT in the neocortex. This is not surprising because approximately 10 to 20 % of patients diagnosed as probable AD reportedly fail to meet pathological criteria for AD at autopsy.

The amnestic subtype of MCI has a high risk of progression to dementia, and it may constitute a prodromal stage of AD [24]. Previous amyloid-PET studies demonstrated a substantial amount of neocortical tracer retention in 50 to 60 % of the MCI population, which is comparable to the level in AD patients [10, 17]. In our study, about half of the MCI patients had elevated neocortical [^{18}F]FACT retention, which was an intermediate level between the aged normal subjects and the AD patients. This finding is in accord with the previous neuropathological observation that the density of neuritic plaque increased as a function of increasing dementia severity [25]. The parent tracer [^{11}C]BF-227 showed neocortical retention to be a reliable indicator of disease progression in MCI subjects in our previous study [17, 19]. Therefore, PET imaging with [^{18}F]FACT is also expected to have a similar prognostic utility.

The amount of elevation of neocortical [^{18}F]FACT uptake in AD patients was approximately 14 to 15 %, far less than PiB and other ^{18}F-labeled amyloid-PET tracers. This is probably due to the relatively low binding affinity and B_{max} of this tracer with amyloid fibrils in comparison to that of PiB (K_d=1.02 nM, B_{max}=0.61) [26, 27]. There is considerable amount of tracer retention in the white matter, which reflects non-specific binding of the compound to myelin sheath. Because of modest specific binding of [^{18}F]FACT in the gray matter of AD patients, spillover from the white matter could reduce the sensitivity for detecting amyloid positive subjects. Use of early phase (30 to 40 min postinjection) images can compensate for this because the relatively stronger signals in the gray matter persist in this time interval. Partial volume correction may also be able to improve the discriminatory power of [^{18}F]FACT-PET by eliminating nonspecific signals in the white matter. Another method to improve the sensitivity for detecting specific signals in the brain is to create a statistical map by comparison with a normal control database [19].

One of advantages of [^{18}F]FACT over BF-227 is its rapid kinetic profile. [^{18}F]FACT showed faster washout from normal brain tissue than BF-227 (Fig. 5) probably because of the lower lipophilicity of FACT (LogP=1.99±0.02) as compared to BF-227 (LogP=2.29±0.02). The neocortical SUVR of [^{18}F]FACT reached a peak at 30 min post-administration. This characteristic would also contribute to reduced procedure and waiting times for PET scans.

Conclusion

We successfully developed a novel ^{18}F-labeled ethenylbenzoxazole derivative, [^{18}F]FACT, as a PET tracer for amyloid deposits. This tracer preferentially bound to dense Aβ plaques in AD brain sections, visualized cortical amyloid deposits in APP Tg mice, and demonstrated fast kinetics and significant retention of [^{18}F]FACT in sites with predilection for the deposition of dense amyloid plaques in AD patients during clinical PET imaging. [^{18}F]FACT PET distinctly distinguished AD patients from normal individuals. These findings suggest that [^{18}F]FACT may be usable for *in vivo* detection of dense Aβ plaques in AD brains.

Acknowledgments. This study was financially supported by the Special Coordination Funds for Promoting Science and Technology, the Health and Labour Sciences Research Grants for Translational research from Ministry of Health, Labour and Welfare, the Program for Promotion of Fundamental Studies in Health Science of the National Institute of Biomedical Innovation, and the Grant-in-Aid for Scientific Research (C) (20591432) from the Ministry of Education, Culture, Sports, Science and Technology of Japan. The authors appreciate the technical assistance of Dr. Shoichi Watanuki in the clinical PET studies.

Conflict of Interest. The authors declare they have no conflicts of interest.

References

1. McKhann GM, Knopman DS, Chertkow H et al (2011) The diagnosis of dementia due to Alzheimer's disease: recommendations from the National Institute on Aging—Alzheimer's Association workgroups on diagnostic guidelines for Alzheimer's disease. Alzheimers Dement 7:263–269
2. Kadir A, Nordberg A (2010) Target-specific PET probes for neurodegenerative disorders related to dementia. J Nucl Med Off Publ Soc Nucl Med 51:1418–1430
3. Furumoto S, Okamura N, Iwata R, Yanai K, Arai H, Kudo Y (2007) Recent advances in the development of amyloid imaging agents. Curr Top Med Chem 7:1773–1789
4. Okamura N, Fodero-Tavoletti MT, Kudo Y et al (2009) Advances in molecular imaging for the diagnosis of dementia. Expert Opin Med Diagn 3:705–716
5. Klunk WE, Engler H, Nordberg A et al (2004) Imaging brain amyloid in Alzheimer's disease with Pittsburgh Compound-B. Ann Neurol 55:306–319
6. Vandenberghe R, Van Laere K, Ivanoiu A et al (2010) ^{18}F-flutemetamol amyloid imaging in Alzheimer disease and mild cognitive impairment: a phase 2 trial. Ann Neurol 68:319–329
7. Barthel H, Gertz HJ, Dresel S et al (2011) Cerebral amyloid-beta PET with florbetaben (^{18}F) in patients with Alzheimer's disease and healthy controls: a multicentre phase 2 diagnostic study. Lancet Neurol 10:424–435
8. Clark CM, Schneider JA, Bedell BJ et al (2011) Use of florbetapir-PET for imaging beta-amyloid pathology. Jama 305:275–283
9. Jureus A, Swahn BM, Sandell J et al (2010) Characterization of AZD4694, a novel fluorinated Abeta plaque neuroimaging PET radioligand. J Neurochem 114:784–794
10. Rowe CC, Ng S, Ackermann U et al (2007) Imaging beta-amyloid burden in aging and dementia. Neurology 68:1718–1725
11. Hatashita S, Yamasaki H (2010) Clinically different stages of Alzheimer's disease associated by amyloid deposition with [^{11}C]-PIB PET imaging. J Alzheimer's Dis JAD 21:995–1003
12. Villemagne VL, Pike KE, Chetelat G et al (2011) Longitudinal assessment of Abeta and cognition in aging and Alzheimer disease. Ann Neurol 69:181–192
13. Dickson TC, Vickers JC (2001) The morphological phenotype of beta-amyloid plaques and associated neuritic changes in Alzheimer's disease. Neuroscience 105:99–107
14. Okamura N, Suemoto T, Shimadzu H et al (2004) Styrylbenzoxazole derivatives for *in vivo* imaging of amyloid plaques in the brain. J Neurosci 24:2535–2541
15. Kudo Y, Okamura N, Furumoto S et al (2007) 2-(2-[2-Dimethylaminothiazol-5-yl]ethenyl)-6- (2-[fluoro]ethoxy)benzoxazole: a novel PET agent for *in vivo* detection of dense amyloid plaques in Alzheimer's disease patients. J Nucl Med 48:553–561
16. Barthel H, Luthardt J, Becker G et al (2011) Individualized quantification of brain beta-amyloid burden: results of a proof of mechanism phase 0 florbetaben PET trial in patients with Alzheimer's disease and healthy controls. Eur J Nucl Med Mol Imaging 38:1702–1714
17. Waragai M, Okamura N, Furukawa K et al (2009) Comparison study of amyloid PET and voxel-based morphometry analysis in mild cognitive impairment and Alzheimer's disease. J Neurol Sci 285:100–108
18. Kudo Y, Furumoto S, Okamura N (2010) Benzoxazole derivatives. US Patent Application 2010/0021385
19. Shao H, Okamura N, Sugi K et al (2010) Voxel-based analysis of amyloid positron emission tomography probe [^{11}C]BF-227 uptake in mild cognitive impairment and Alzheimer's disease. Dement Geriatr Cogn Disord 30:101–111
20. McKhann G, Drachman D, Folstein M, Katzman R, Price D, Stadlan EM (1984) Clinical diagnosis of Alzheimer's disease: report of the NINCDS-ADRDA Work Group under the auspices of Department of Health and Human Services Task Force on Alzheimer's Disease. Neurology 34:939–944
21. Petersen RC, Smith GE, Waring SC, Ivnik RJ, Tangalos EG, Kokmen E (1999) Mild cognitive impairment: clinical characterization and outcome. Arch Neurol 56:303–308
22. Okamura N, Shiga Y, Furumoto S et al (2009) *In vivo* detection of prion amyloid plaques using [^{11}C]BF-227 PET. Eur J Nucl Med Mol Imaging 37:934–941
23. Kikuchi A, Takeda A, Okamura N et al (2010) *In vivo* visualization of alpha-synuclein deposition by carbon-11-labelled 2-[2-(2-dimethylaminothiazol-5-yl)ethenyl]-6-[2-(fluoro)ethoxy]benzoxazole positron emission tomography in multiple system atrophy. Brain J Neurol 133:1772–1778
24. Gauthier S, Reisberg B, Zaudig M et al (2006) Mild cognitive impairment. Lancet 367:1262–1270
25. Haroutunian V, Perl DP, Purohit DP et al (1998) Regional distribution of neuritic plaques in the nondemented elderly and subjects with very mild Alzheimer disease. Arch Neurol 55:1185–1191
26. Fodero-Tavoletti MT, Mulligan RS, Okamura N et al (2009) *In vitro* characterisation of BF227 binding to alpha-synuclein/Lewy bodies. Eur J Pharmacol 617:54–58
27. Fodero-Tavoletti MT, Smith DP, McLean CA et al (2007) *In vitro* characterization of Pittsburgh compound-B binding to Lewy bodies. J Neurosci Off J Soc Neurosci 27:10365–10371

Shidahara et al. EJNMMI Research 2013, 3:32
http://www.ejnmmires.com/content/3/1/32

EJNMMI Research
a SpringerOpen Journal

ORIGINAL RESEARCH Open Access

Evaluation of the biodistribution and radiation dosimetry of the ^{18}F-labelled amyloid imaging probe [^{18}F]FACT in humans

Miho Shidahara[1,2*], Manabu Tashiro[2], Nobuyuki Okamura[3], Shozo Furumoto[3], Katsutoshi Furukawa[4], Shoichi Watanuki[2], Kotaro Hiraoka[2], Masayasu Miyake[2], Ren Iwata[5], Hajime Tamura[1], Hiroyuki Arai[4], Yukitsuka Kudo[6] and Kazuhiko Yanai[2,3]

Abstract

Background: The biodistribution and radiation dosimetry of the ^{18}F-labelled amyloid imaging probe ([^{18}F] FACT) was investigated in humans.

Methods: Six healthy subjects (three males and three females) were enrolled in this study. An average of 160.8 MBq of [^{18}F] FACT was intravenously administered, and then a series of whole-body PET scans were performed. Nineteen male and 20 female source organs, and the remainder of the body, were studied to estimate time-integrated activity coefficients. The mean absorbed dose in each target organ and the effective dose were estimated from the time-integrated activity coefficients in the source organs. Biodistribution data from [^{18}F] FACT in mice were also used to estimate absorbed doses and the effective dose in human subjects; this was compared with doses of [^{18}F] FACT estimated from human PET data.

Results: The highest mean absorbed doses estimated using human PET data were observed in the gallbladder (333 ± 251 μGy/MBq), liver (77.5 ± 14.5 μGy/MBq), small intestine (33.6 ± 30.7 μGy/MBq), upper large intestine (29.8 ± 15.0 μGy/MBq) and lower large intestine (25.2 ± 12.6 μGy/MBq). The average effective dose estimated from human PET data was 18.6 ± 3.74 μSv/MBq. The highest mean absorbed dose value estimated from the mouse data was observed in the small intestine (38.5 μGy/MBq), liver (25.5 μGy/MBq) and urinary bladder wall (43.1 μGy/MBq). The effective dose estimated from the mouse data was 14.8 μSv/MBq for [^{18}F] FACT.

Conclusions: The estimated effective dose from the human PET data indicated that the [^{18}F] FACT PET study was acceptable for clinical purposes.

Keywords: Positron emission tomography, Radiation dosimetry, Amyloid imaging, MIRD, [^{18}F] FACT

Background

Amyloid beta imaging

Deposits of amyloid β (Aβ) plaque are one of the pathological observations in patients with Alzheimer's disease (AD); Aβ deposition progresses at an earlier point than the current clinical diagnostic point for this disease [1]. For earlier diagnosis of AD and the evaluation of treatment efficacy, *in vivo* amyloid imaging using positron emission tomography (PET), which provides quantitation and visualisation of Aβ deposition in the brain, is useful. Therefore, several Aβ-binding probes dedicated for PET imaging have been developed [2,3].

Most of these PET Aβ ligands are ^{11}C-labelled compounds (physical half life ($T_{1/2}$), 20 min), and ^{18}F-labelled agents are being increasingly investigated owing to their long half life ($T_{1/2}$, 109.7 min). The long $T_{1/2}$ of ^{18}F enables several PET scans to be carried out from a single synthesis of labelled agent and also enables its commercial distribution to any PET facility. On the other hand, the longer the $T_{1/2}$ of the radioisotope gets, the greater is the radiation

* Correspondence: shidahara@med.tohoku.ac.jp
[1]Division of Medical Physics, Tohoku University School of Medicine, 2-1 Seiryo-machi, Aoba-ku, Sendai 980-8575, Japan
[2]Division of Cyclotron Nuclear Medicine, Cyclotron Radioisotope Center, Tohoku University, Sendai 980-8578, Japan
Full list of author information is available at the end of the article

dose exposure for the PET subject for the same administered dose of radioligand.

Importance of radiation dosimetry

For subjects undergoing PET, internal radiation exposure is inevitable, and the radiation dose delivered is proportional to the level of radioactivity of the injected radioligand and the number of injections. In the case of amyloid imaging, subjects often have multiple PET scans for diagnostic or therapeutic longitudinal monitoring of Aβ aggregation in the brain. Therefore, estimation of the radiation dose exposure from each PET radioligand and the use of well-balanced PET scan protocols taking into consideration subject risk and benefit are important.

Estimation of the internal radiation dose requires a time series measurement of the biodistribution of the injected radioligand. There are two ways to establish the biodistribution of a radioligand in humans: one is to extrapolate from data obtained in animal experiments [4] and the other is to use data from a clinical whole-body PET study [5]. Data extrapolated from animal experiments have been used to estimate clinical radiation dose. However, Sakata et al. reported that in some radioligands, there were considerable differences in organ dose or kinetics between human and animal experiments and that a whole-body PET study would be desirable for the initial clinical evaluation of new PET radioligands [6].

Previous biodistribution and dosimetry study for PET amyloid imaging

Recently, radiation dose exposures from several PET amyloid imaging agents have been reported using clinical whole-body PET scans. One of the popular amyloid ligands, Pittsburgh compound B ([^{11}C]PIB), has been extensively investigated with regard to its kinetics in the human body, and its effective radiation dose was found to be 4.74 μSv/MBq on average [7]. For ^{18}F-labelled PET amyloid radioligands, effective doses in humans have been reported as follows: ^{18}F-AV-45, 13 and 19.3 μSv/MBq [8,9]; ^{18}F-GE067, 33.8 μSv/MBq [10]; and ^{18}F-BAY94-9172, 14.7 μSv/MBq [11].

Aim of the present study

Fluorinated amyloid imaging compound ([^{18}F]FACT) is an ^{18}F-labelled amyloid imaging agent developed at Tohoku University [12]. Kudo and colleagues at this university have previously developed a ^{11}C amyloid imaging agent named [^{11}C]BF-227 [3]. [^{18}F]FACT is derived from [^{11}C]BF-227 by reducing its lipophilicity in order to reduce the nonspecific binding in the brain; AD patients showed significantly higher uptake of [^{18}F]FACT in the neocortex region relative to controls [12]. However, the biodistribution of [^{18}F]FACT in humans has not yet been investigated.

In the present study, the radiation dosimetry and biodistribution of [^{18}F]FACT was investigated in healthy elderly subjects who are the target group for PET amyloid imaging. In order to determine the discrepancy in the estimated radiation dose between human and animal experiments, biodistribution studies in mice involving [^{18}F]FACT were also conducted.

Methods

Subjects

PET studies were performed in three healthy male and in three healthy female volunteers (mean age ± standard deviation (SD), 76.3 ± 3.2 years). Subject characteristics are shown in Table 1. Both height and weight varied over a wide range (146 to 175 cm and 39 to 74 kg, respectively). All subjects were Japanese and were free of somatic and neuropsychiatric illness, as determined by clinical history and physical examination; one male subject (no. 1) had undergone a previous surgical operation involving gallbladder removal.

This study was approved by the Ethics Committee on Clinical Investigations of Tohoku University School of Medicine and was performed in accordance with the Declaration of Helsinki. Written informed consent was obtained from all subjects after a complete description of the study had been made.

Radiochemistry and radioligand purity

Figure 1 shows the chemical structure of ^{18}F-FACT. The radiochemical purity of the radioligand in the present clinical study ranged from 97.8% to 98.7% (mean ± SD, 98.33 ± 0.42%). The specific radioactivity ranged from 30.6 to 347.7 GBq/μmol at the time of injection (mean ± SD, 139.9 ± 116.2 GBq/μmol).

PET study

All whole-body PET studies were performed using a SET-2400W scanner (Shimadzu Inc., Kyoto, Japan) in two-dimensional (2D) mode [13]. The PET scanner acquired 63 image slices at a centre-to-centre interval of 3.125 mm and had a spatial resolution of 3.9 mm full width at half maximum (FWHM) and a *Z*-axis resolution of 6.5 mm FWHM at centre field of view [13].

An overview of scan protocols is shown in Figure 2. Four emission scans and two transmission scans (before administration and intermediate emission scans) using a ^{68}Ge/^{68}Ga source were performed, with the exception of subject no. 1 who had three emission scans. In the present series of PET studies and in other research projects, a 15-min PET brain scan using three-dimensional (3D) mode was performed after the first emission scan. At 2 min after intravenous administration of 142 to 180 MBq [^{18}F]FACT (mean ± SD, 160.8 ± 14.8 MBq; injection mass, 0.77 ± 0.66 ng), a series of whole-body PET